The Impact of Scaling Training Data on Adversarial Robustness

Marco Zimmerli
ETH Zürich
mzimmerli@ethz.ch

Andreas Plesner
ETH Zürich
aplesner@ethz.ch

Till Aczel
ETH Zürich
taczel@ethz.ch

Roger Wattenhofer
ETH Zürich
wattenhofer@ethz.ch

Abstract

Deep neural networks remain vulnerable to adversarial examples despite advances in architectures and training paradigms. We investigate how training data characteristics affect adversarial robustness across 36 state-of-the-art vision models spanning supervised, self-supervised, and contrastive learning approaches, trained on datasets from 1.2M to 22B images. Models were evaluated under six black-box attack categories: random perturbations, two types of geometric masks, COCO object manipulations, ImageNet-C corruptions, and ImageNet-R style shifts. Robustness follows a logarithmic scaling law with both data volume and model size: a tenfold increase in data reduces attack success rate (ASR) on average by 3.2%, whereas a tenfold increase in model size reduces ASR on average by 13.4%. Notably, some self-supervised models trained on curated datasets, such as DINOv2, outperform others trained on much larger but less curated datasets, challenging the assumption that scale alone drives robustness. Adversarial fine-tuning of ResNet50s improves generalization across structural variations but not across color distributions. Human evaluation reveals persistent gaps between human and machine vision. These results show that while scaling improves robustness, data quality, architecture, and training objectives play a more decisive role than raw scale in achieving broad-spectrum adversarial resilience.

1 Introduction

Deep neural networks have achieved remarkable success in computer vision tasks [31, 44, 32, 20, 40]. Yet, their vulnerability to adversarial examples remains a fundamental challenge to their deployment in safety-critical applications [48]. Adversarial examples are inputs with semantic preserving changes that cause misclassifications, revealing a significant gap between human and machine perception [17]. While humans recognize objects under various distortions, state-of-the-art models can be fooled by imperceptible modifications [48, 38]. This vulnerability raises profound questions about the nature of learned representations and the factors that determine model robustness.

The asymmetry between human and machine perception creates critical security vulnerabilities across deployed systems. In visual domains, adversarial perturbations that remain imperceptible or semantically clear to humans can cause catastrophic failures in machine vision applications. Content moderation systems exemplify this vulnerability, where malicious actors can craft adversarial examples to evade automated filters while the harmful content remains readily identifiable to human observers [1, 46]. Similarly, autonomous vehicle perception systems can be manipulated through

39th Conference on Neural Information Processing Systems (NeurIPS 2025) Workshop: Reliable ML from Unreliable Data.

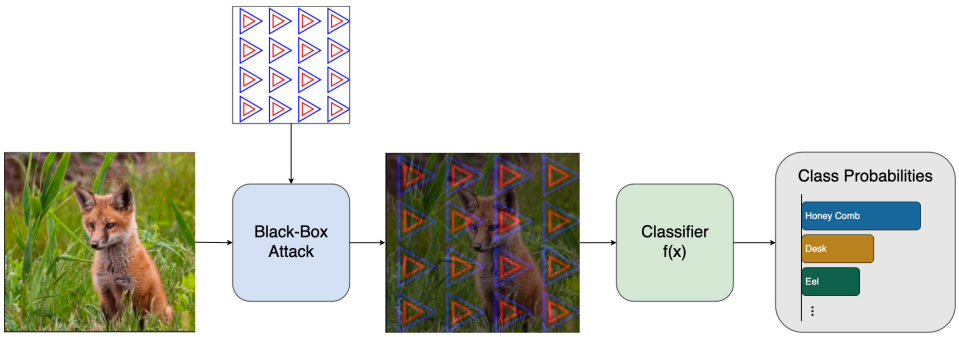

Figure 1: Overview of the black-box attack pipeline. Input images are modified using a semantic adversarial attack. In this example, an ImageNet image of a red fox is attacked using the GeometricMasksV2 3-4-2 C1 with an opacity of 128, causing a misclassification in the target classifier.

carefully designed perturbations that preserve semantic meaning for human drivers but induce misclassifications in computer vision models [8]. These vulnerabilities extend beyond visual tasks, as analogous techniques compromise malware detection and other pattern recognition systems [18, 5]. The fundamental gap in robustness between biological and artificial perception thus constitutes a systematic attack surface rather than merely a theoretical limitation.

Recent advances in vision model architectures have produced increasingly sophisticated systems, from Vision Transformers [14] to self-supervised models like DINOv2 [37] and multi-modal architectures such as CLIP [41]. These models employ fundamentally different training paradigms, namely supervised, self-supervised, and contrastive learning, and are trained on datasets of unprecedented scale that range from millions to billions of images. While conventional wisdom suggests that larger datasets and more sophisticated training objectives should confer greater robustness, empirical evidence reveals a more nuanced reality. The interplay between data quantity, curation quality, and training paradigm produces unexpected robustness patterns, with some smaller, carefully curated datasets yielding models more robust than those trained on orders of magnitude more data [12, 27]. Despite extensive research on individual factors, the relationship between these training characteristics and resulting adversarial robustness remains poorly understood.

This work investigates how training data shapes adversarial robustness in vision models. We systematically evaluate 36 state-of-the-art image classification models across six distinct black-box attack categories, ranging from simple color perturbations to complex geometric occlusions and artistic domain shifts. Our analysis spans models trained on datasets from 1.2 million to 22 billion images, enabling insights into scaling laws for adversarial robustness. An overview of our attack pipeline can be found in Figure 1. We address four central research questions:

1. Does training data scale influence model vulnerability to different adversarial perturbations?
2. Do self-supervised and contrastive learning paradigms inherently produce more robust representations than supervised training?
3. Despite targeted adversarial training, can novel geometric mask configurations always be constructed to exploit vulnerabilities in fine-tuned models?
4. Can adversarial fine-tuning align model robustness with human perceptual invariance?

Our investigation employs a comprehensive black-box evaluation framework that emphasizes semantic validity over bounded perturbations [38]. Unlike traditional ℓ_p-norm constrained attacks [17, 36], we focus on perturbations that preserve semantic content while exploiting model vulnerabilities, such as geometric masks [30], artistic renditions [23], and naturalistic corruptions [22].

Our work makes four principal contributions to understanding adversarial robustness. First, we establish quantitative scaling laws demonstrating that robustness improvements saturate logarithmically with training data volume. Additionally, attack-specific variations reveal fundamental differences in how models handle spatial versus stylistic perturbations. We further find that scale without quality control offers minimal benefits for CLIP models, indicating that strategic data curation supersedes volume for comprehensive adversarial robustness. Second, we show that the training paradigm has

minimal impact on robustness compared to data curation quality and model scale. Third, through targeted adversarial fine-tuning experiments with geometric masks, we demonstrate that ResNet50 models can learn robust features that generalize across structural variations but fail to transfer across color distributions. Fourth, our human evaluation studies reveal persistent gaps between human and machine vision, with even the best models exhibiting vulnerabilities that humans navigate effortlessly.

2 Related Work

Adversarial Examples and Attack Methods The vulnerability of neural networks to adversarial examples has been a central concern since their discovery [48, 5]. These imperceptible perturbations, which cause misclassifications, have driven the development of increasingly effective attacks. The Fast Gradient Sign Method (FGSM) introduced an efficient single-step gradient ascent approach [17], followed by iterative methods such as Projected Gradient Descent (PGD) for stronger attacks [36]. The AutoAttack framework unified multiple complementary attacks into a parameter-free benchmark for reliable, reproducible evaluation [10]. It is also the default evaluation method in RobustBench, which ranks models for consistent, reproducible robustness comparisons [11].

Beyond small ℓ_p-bounded perturbations, researchers have explored semantic adversarial examples that preserve image meaning while drastically altering model predictions. State-of-the-art models turn out to be vulnerable to comparably natural classes of perturbations like translations and rotations [15]. Research on semantic adversarial examples introduced HSV color space transformations, demonstrating that shifting hue and saturation components while preserving brightness can reduce CNN accuracy to below 10% on CIFAR-10 [25]. This approach exploits the shape bias of human vision, generating naturally appearing images that contain the original object with different colors. Recent work on Generative Adversarial Training (GAT) and composite adversarial attacks builds on these ideas by integrating multiple semantic perturbations, such as hue, saturation, brightness, contrast, and rotation, to construct more comprehensive threat models [28].

Defense Mechanisms Adversarial training has emerged as the predominant defense mechanism due to its conceptual simplicity and empirical effectiveness [36, 17]. This approach incorporates adversarially perturbed examples during training to improve model robustness. Recent advances have demonstrated that adversarial training benefits substantially from increased training data volume, exceptionally high-quality synthetic data [42].

Data Distribution and Robustness Sensitivity A critical finding in adversarial robustness research concerns the sensitivity of robust accuracy to input data distributions. It has been demonstrated that semantically-preserving transformations of data distributions can drastically alter the adversarial robustness of models, even when retrained on the transformed distribution [12].

Scaling Trends in Adversarial Robustness CIFAR-10 adversarial robustness has been studied by training WideResNets with large synthetic datasets and evaluating under white-box conditions using AutoAttack and 40-step PGD on the models' CW loss, showing that robustness scales with model and dataset size but plateaus near 90% accuracy, partly due to invalid adversarial images that also fool humans[3]. Recent investigations into scaling laws for adversarial robustness of language models reveal that, unlike standard accuracy, larger language models do not consistently exhibit improved robustness [27]. In the same line of work, offense-defense balance analyses indicate that increasing attack compute currently outpaces defense improvements for fixed model sizes. However, larger models exhibit more favorable defense scaling properties, hinting that scaling model capacity may eventually shift the advantage toward defense [27]. Further, it has been shown that larger models generally achieve higher ℓ_∞-robust accuracy under the AutoAttack on ImageNet [47].

Synthetic Data Quality and Training Efficiency The quality of synthetic training data, often measured through Fréchet Inception Distance (FID) [24], has a significant impact on adversarial robustness outcomes [3]. Recent work has incorporated data quality metrics into scaling laws, demonstrating that higher-quality synthetic data enables more compute-efficient adversarial training. In contrast, low-quality data limits the benefits of scaling [3].

3 Experimental Design for Robustness Scaling Analysis

3.1 Model Setup

The analysis was carried out on ViT [14], ResNet [19], CLIP [41], DINOv1 [7], DINOv2 [37], Swin [33], Swinv2 [34], ConvNeXt [35], YOLO [50], ViT-MAE [21], PaliGemma [4], BEiT [2], BEiTv2 [39], SigLIP [51] and SigLIPv2 [49] models, where the exact specifications can be found in the Appendix Table 2. All models in this study were evaluated on the ImageNet-1K classification task (validation split) for benchmarking image recognition [45]. Each model utilized its standard preprocessing transformations during evaluation.

CLIP models were evaluated in a zero-shot classification setting without additional training, using prompts of the form "a photo of a {class name}" for each of the 1,000 ImageNet classes, following standard CLIP evaluation protocols [41]. All variants use the OpenCLIP framework [9], except for the Apple DFN CLIP models [16], which were loaded from the Hugging Face model repository.

DINOv1, ViT-MAE, and PaliGemma were not initially designed for ImageNet classification, so a single linear classification head was appended to the frozen backbone features. The backbone was frozen while only the classification head was trained on the ImageNet training split using Cross-Entropy Loss. The exact training specifications can be found in the Appendix Table 3.

3.2 Evaluation Metrics

Following Dong et al. [13], we evaluate models using accuracy and attack success rate (ASR). Let $\mathcal{D} = \{(x_i, y_i)\}_{i=1}^{N}$ be a dataset of N image-label pairs, where x_i is an input sample and y_i its corresponding ground-truth label. We write $C(\cdot)$ for a classifier and $A(\cdot)$ for an adversarial attack.

Accuracy The accuracy of a classifier C on a dataset $\mathcal{D}$ is defined as

$$\text{Acc}(C, \mathcal{D}) = \frac{1}{|\mathcal{D}|} \sum_{(x,y)\in\mathcal{D}} \mathbf{1}[C(x) = y], \quad \mathbf{1}[\cdot] \text{ is the indicator function.}$$

Attack Success Rate (ASR) ASR is defined as the ratio of initially correctly classified images that become misclassified after applying the adversarial attack. Let $\mathcal{S}_{\text{correct}} = \{(x, y) \in \mathcal{D}_{\text{clean}} \mid C(x) = y\}$ be the subset of correctly classified images by classifier C from the clean dataset $\mathcal{D}_{\text{clean}}$. Then

$$\text{ASR}(C, A, \mathcal{S}_{\text{correct}}) = \frac{1}{|\mathcal{S}_{\text{correct}}|} \sum_{(x,y)\in\mathcal{S}_{\text{correct}}} \mathbf{1}[C(A(x)) \neq y].$$

Approximation of Attack Success Rate For certain attack scenarios where only the adversarially attacked dataset $\mathcal{D}_{\text{adv}} = \{(A(x_i), y_i)\}_{i=1}^{N}$ is available, we approximate the ASR using a surrogate clean dataset $\mathcal{D}_{\text{surrogate}} = \{(x_i^{\text{sur}}, y_i^{\text{sur}})\}_{i=1}^{M}$ that resembles the unavailable original $\mathcal{D}_{\text{clean}}$. The approximated ASR is computed as

$$\text{ASR}_{\text{approx}}(C, \mathcal{D}_{\text{adv}}, \mathcal{D}_{\text{surrogate}}) = \frac{\text{Acc}(C, \mathcal{D}_{\text{surrogate}}) - \text{Acc}(C, \mathcal{D}_{\text{adv}})}{\text{Acc}(C, \mathcal{D}_{\text{surrogate}})}.$$

To validate this approximation, we evaluated all 36 models on all 19 attacks for which both clean and adversarial images are available, and compared the resulting approximated and actual ASR values. The approximation systematically underestimated the actual ASR by an average of 3.09%-points ($\sigma = 1.93\%$-points), computed over all 684 evaluation points (36 models × 19 attacks). This underestimation occurs because the approximation cannot account for initially misclassified samples that become correctly classified under adversarial perturbation, a phenomenon that reduces the apparent accuracy drop. Despite this bias, the approximation provides consistent relative rankings across models, enabling meaningful comparative analysis when actual ASR computation is infeasible.

3.3 Attacks

We consider a black-box threat model in which adversaries have no access to the model's architecture, parameters, or gradients [38]. Moreover, we impose no constraints on the perturbation magnitude,

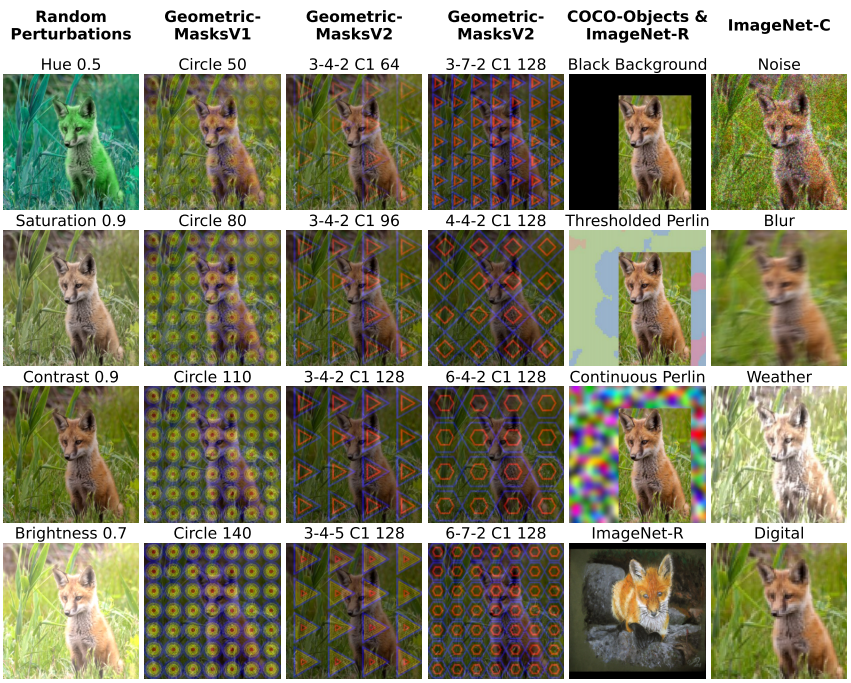

Figure 2: Sample images of all attacks applied for the robustness analysis of the categories Random Perturbations, GeometricMasksV1, GeometricMasksV2, COCO-Objects, ImageNet-R, and ImageNet-C. The original image is from the ImageNet class red fox.

thereby enabling exploration of a broader range of attack strategies, including those that introduce perceptible yet semantically consistent perturbations [30]. Figure 2 shows a sample for every attack applied in the robustness analysis, while further sample images are available in Appendix C. We provide descriptions of the attacks in Appendix B.

4 Adversarial Fine-Tuning

To investigate the relationship between adversarial training and model generalization capabilities, we fine-tuned three ResNet50 models using different GeometricMasksV2 configurations. These experiments assess whether models can learn robust features from structured adversarial examples and generalize beyond the specific perturbations encountered during training. Each model was initialized from ImageNet pre-trained weights and fine-tuned on a modified version of the ImageNet training set, where a controlled percentage of images were augmented using the GeometricMasksV2 attack. The fine-tuning process targeted all model parameters while maintaining the original architecture.

Following fine-tuning, the models underwent evaluation on various GeometricMasksV2-based adversarial attacks, including a novel color scheme, C3, and a 45-degree rotated mask, named C4. Examples of all the GeometricMasksV2 applied in this evaluation can be found in Figure 13 with more in Appendix D.

Table 1: Fine-tuning configurations for ResNet50 models with GeometricMasksV2 augmentation. All models were trained with a batch size of 64 for three epochs.

Model Variant	Mask Type	Color Scheme	Opacity	Adversarial Examples
ResNet50-v1	3-4-2	C1	64	50%
ResNet50-v2	3-4-2	C1 & C2	64	50%
ResNet50-v3	Random	C1 & C2	64	50%

5 Human-Model Alignment

The human evaluation employed the GeometricMasksV2 attack with configuration 6-7-2 C1, identified in our robustness analysis as producing the highest attack success rates for some of the evaluated models. This evaluation serves not only to assess the attack's effectiveness on humans but also to confirm that it continues to produce valid semantic adversarial examples. The geometric mask was applied to the ImageNette dataset, a curated subset of ImageNet comprising ten visually distinct classes [26]. It provides a simplified classification task well-suited for human participants. The evaluation protocol consisted of:

- **Dataset**: 25 randomly selected ImageNette images per difficulty level
- **Task**: 10-way classification among ImageNette categories without time constraints
- **Perturbation**: GeometricMasksV2 (6-7-2 C1)
- **Difficulty** levels:
  - Baseline: Opacity 0 (no occlusion)
  - Easy: Opacity 64 (minimal occlusion)
  - Medium: Opacity 96 (moderate occlusion)
  - Hard: Opacity 128 (substantial occlusion)

The graphical user interface employed in the evaluation is illustrated in Appendix Figure 15. A total of six human participants completed the evaluation protocol, and we report the mean accuracy for each difficulty level across these individuals. In parallel, five models were evaluated on the complete ImageNette dataset, including the adversarially fine-tuned ResNet50-v1 described in Section 4. For a fair comparison with human participants, model predictions were restricted to the ten ImageNette classes. This experimental design enables a direct comparison between human and model performance across difficulty levels. The results confirm the validity of the adversarial examples as human participants consistently achieved accuracies exceeding 93% at all difficulty levels. While the adversarially fine-tuned ResNet50-v1 showed substantially improved robustness, the other model's performance often deteriorated significantly starting at the easy level.

6 Results

6.1 Robustness Scaling Analysis

Due to space, some results are moved to Appendix G. For instance, results show that contrastive learning shows the lowest average ASR at 27.9%, while self-supervised learning is at 28.4%, and supervised learning has the highest vulnerability with 34.3% ASR on average.

6.1.1 Datasets and Adversarial Robustness

Figure 3 presents the comprehensive robustness evaluation across all attack categories using the overall average attack success rate. This metric is calculated as the mean of the average ASR values for each attack category: Random Perturbations, GeometricMasksV1, GeometricMasksV2, COCO Objects, ImageNet-C, and ImageNet-R. It provides a holistic assessment of model vulnerability. Lower ASR values indicate superior robustness across diverse adversarial conditions.

The relationship between training data scale and overall robustness follows a logarithmic function: $ASR = -3.16 \log_{10}(x) + 55.53$, where x represents the training dataset size in number of images. This enhanced scaling coefficient suggests that increased training data provides cumulative benefits across multiple robustness dimensions rather than specialized defenses against specific perturbations. Note that this scaling law does not account for the correlation of 0.59 between dataset size and model size. See Section 6.1.3 for a scaling law with separated training data size and model size.

CLIP models do not follow the scaling trend as closely as expected. Despite some top performers like CLIP-EVA02-L-14, most models underperform given their training data scale, especially the smallest architecture, CLIP-ViT-B-32. The degraded performance presumably occurs due to the lower training data quality in the web-collected image-text pairs. This implies that scale without quality control offers minimal benefits, indicating that strategic data curation supersedes volume for comprehensive

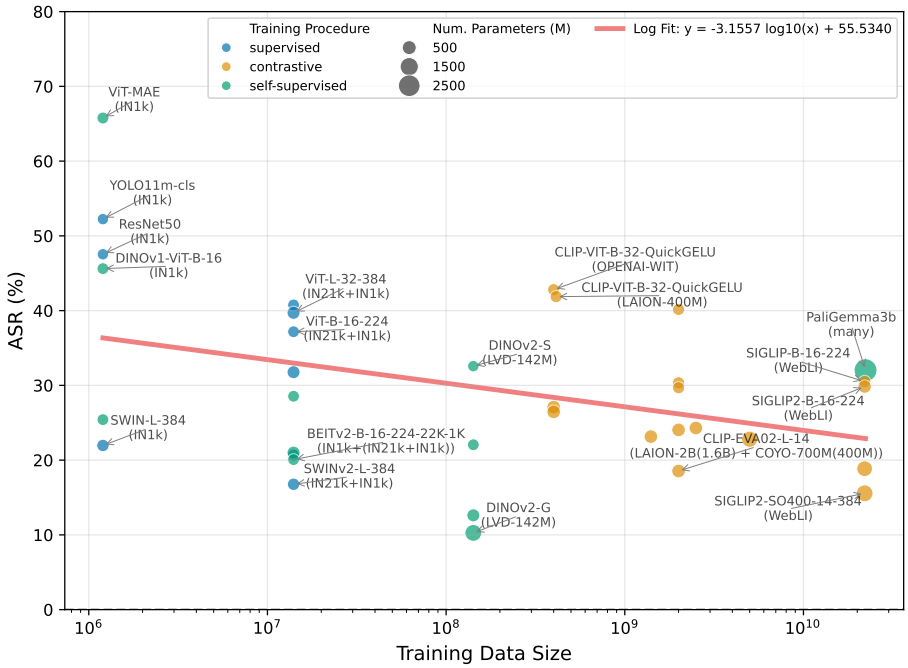

Figure 3: Overall average ASR across different attack categories: Random Perturbations, GeometricMasksV1, GeometricMasksV2, COCO Objects, ImageNet-C, and ImageNet-R. The overall average is computed as the mean of the average ASR values for each attack category. We show in Figure 16 the same plot with labels for all points.

adversarial robustness. Notably, for a given CLIP architecture, models almost always exhibit superior robustness when trained on larger datasets. In Appendix F.1, we provide a detailed comparison of four CLIP-ViT-L-14 models.

Self-supervised DINOv2 models dominate the low-ASR regime. DINOv2-G achieves the lowest overall ASR at 10.3%, closely followed by DINOv2-L, establishing a clear performance hierarchy within the DINOv2 family that correlates with model scale. This consistent scaling behavior, also observed for other architectures, indicates that an increase in model size can improve the robustness within a model family.

Web-scale trained models occupy the second tier of performance. The SigLIP-SO400 and SigLIP2-SO400 variants, trained on WebLI with roughly 155 times more data than DINOv2, achieve ASRs that nearly match those of DINOv2-G despite employing fundamentally different training paradigms.

Traditional supervised models show a significant variance in the vulnerability across the evaluation suite. ResNet50 and YOLO11m-cls occupy the high-ASR region. Swin-L-384 achieves a comparable ASR despite only training on ImageNet-1K. Swinv2-L-384 further improves with an updated architecture and additional training on ImageNet-21K, achieving a superb ASR of 16.8%. The performance of the Swin models indicates that the architecture and the training procedure may compensate for their small training datasets.

6.1.2 Model Scale and Adversarial Robustness

We find the relationship between model size and adversarial robustness reveals a consistent scaling law as shown in Figure 4, with attack success rates decreasing logarithmically as model parameters increase. Larger models exhibit significantly reduced vulnerability to adversarial perturbations, following the relationship $ASR = -13.39 \log_{10}(x) + 141.18$. This robust scaling behavior spans multiple orders of magnitude, from compact models like ResNet50 with high ASRs approaching 50%, to massive architectures such as DINOv2-G achieving ASRs below 15%. The logarithmic nature of this relationship suggests small returns as model scale increases. Yet, the consistent downward trend across diverse architectures and training paradigms indicates that increased parameter count provides a fundamental defensive advantage against adversarial attacks. Notably, this size-robustness

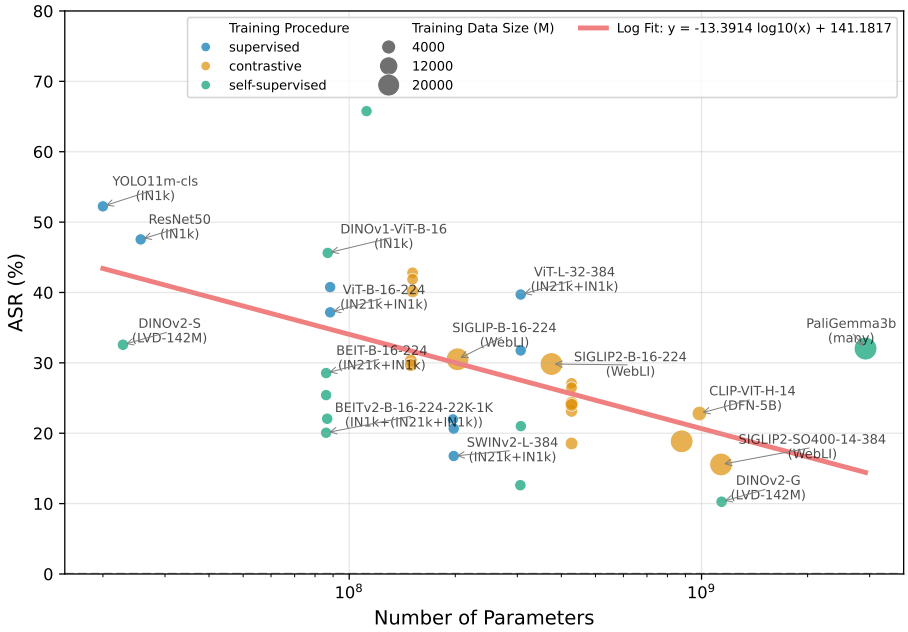

Figure 4: Overall average ASR relative to the number of model parameters averaged across: Random Perturbation, GeometricMasksV1, GeometricMasksV2, Coco Objects, ImageNet-C, and ImageNet-R attacks. We show in Figure 17 the same plot with labels for all points.

correlation appears largely independent of training methodology, as models of similar scale cluster together despite employing different learning objectives, suggesting that the sheer capacity to learn complex representations may be more critical for adversarial robustness than the specific training approach.

6.1.3 Fitting a Two-Variable Scaling Law for ASR

The univariate scaling laws presented above do not consider the correlation between training dataset size and model size, which in our data is 0.59. This correlation reflects the common practice that larger models are typically trained on larger datasets. Ignoring this relationship can bias the interpretation of how each factor independently influences attack success rate (ASR).

To account for the joint effect of dataset and model size, we computed a bivariate scaling law. To make this relationship separable, so that the contributions of training dataset size and model size can be individually assessed, we applied principal component analysis (PCA) to the log-transformed data. We then fitted a linear function in the PCA space and projected the result back to the original variables. The resulting bivariate scaling law is:

$$\text{ASR} = -0.46 \log_{10}(x_{data}) - 12.53 \log_{10}(x_{model}) + 137.67$$

where x_{data} is the training dataset size and x_{model} is the model size. This result indicates that model size has a more pronounced effect on ASR than dataset size. Both univariate and bivariate approaches have their validity. While the implicit correlation can influence the univariate scaling law, since larger models tend to be trained on larger datasets, the bivariate law allows us to separate these effects. Nevertheless, in practice, one cannot train huge models on small datasets and vice versa, so the univariate scaling law still provides relevant insights in realistic training regimes.

While the model size shows better scaling, the data scaling can be beneficial as it does not impact inference costs.

6.2 Human-Model Alignment

Figure 5 presents the comparative evaluation of human and model performance on ImageNette under GeometricMasksV2 (6-7-2 C1) perturbations at varying opacity levels. The baseline (opacity 0) represents unperturbed ImageNette images, where all achieve near-perfect accuracy.

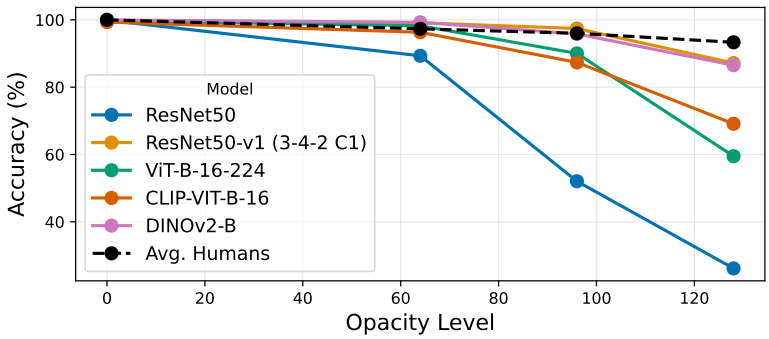

Figure 5: Accuracies of various models and the average accuracy of human participants on the GeometricMasksV2 6-7-2 C1 mask, applied at opacities 0, 64, 96, and 128. Raw values in Table 6.

Human participants demonstrate superior robustness across all opacity levels. The gradual degradation of the human participants' accuracy contrasts sharply with the steeper performance declines observed in computational models, showing that model limitations cause the performance drops.

The fine-tuned ResNet50 (ResNet-v1) and DINOv2-B perform the closest to humans. The models demonstrate that appropriate training strategies, whether through adversarial fine-tuning or self-supervised learning, can substantially enhance robustness to geometric perturbations.

The models ViT-B-16-224 and CLIP-VIT-B-16 display similar performance profiles through moderate perturbation levels, but drop significantly after opacity 64. This performance cliff indicates a fundamental limitation in handling severe geometric occlusions despite robustness to mild perturbations.

The vanilla ResNet50 demonstrates pronounced vulnerability even at minimal perturbation levels. This performance pattern underscores the critical importance of specialized training, as the identical architecture achieves near-human robustness when fine-tuned with geometric masks.

These results establish that humans are more robust than models. Further, the results demonstrate that the mask 6-7-2 C1, the most severe attack in GeometricMasksV2, renders valid adversarial examples even at opacity 128. The persistent gap between human and model performance, particularly at high opacity levels, reveals a fundamental vulnerability that can be exploited in adversarial settings. At opacity 128, even the best-performing models misclassified approximately 13% of images that humans correctly identify, demonstrating that carefully crafted perturbations can selectively impair machine vision while preserving human interpretability. This asymmetry highlights the differences in robustness mechanisms between biological and artificial vision systems.

7 Conclusion

Our evaluation of 36 vision models reveals that adversarial robustness is governed by clear, logarithmic scaling laws concerning model *and* dataset size. The relationship for training data is $ASR = -3.1557 \log_{10}(x) + 55.5340$, and for model size is $ASR = -13.3914 \log_{10}(x) + 141.1817$. However, scale is not the sole determinant of resilience. The superior performance of models like DINOv2, trained on highly curated data, indicates that quality can be more impactful than sheer volume. We found that the training paradigm—supervised, self-supervised, or contrastive—has a limited effect on robustness, suggesting architectural and data characteristics are more critical.

Adversarial fine-tuning on geometric masks confirmed that models can learn to generalize across structural variations like shape, scale, and rotation. However, this robustness is brittle and fails to transfer to unseen color schemes, indicating that geometric and chromatic invariance are learned separately. Furthermore, human evaluators consistently outperformed all models, including fine-tuned ones, highlighting a persistent and fundamental gap between biological and artificial visual systems.

Our study is limited by the lack of standardized dataset documentation and a focus on black-box attacks. Future work should expand the attack taxonomy to include gradient-based methods to test if these scaling trends hold. Extending evaluations to tasks like object detection and segmentation would further clarify how data and model scale influence robustness in scenarios requiring complex spatial reasoning.

References

[1] Piush Aggarwal, Pranit Chawla, Mithun Das, Punyajoy Saha, Binny Mathew, Torsten Zesch, and Animesh Mukherjee. Hateproof: Are hateful meme detection systems really robust? In *Proceedings of the ACM Web Conference 2023*, WWW '23, page 3734–3743, New York, NY, USA, 2023. Association for Computing Machinery. ISBN 9781450394161. doi: 10.1145/3543507.3583356. URL https://doi.org/10.1145/3543507.3583356.

[2] Hangbo Bao, Li Dong, Songhao Piao, and Furu Wei. Beit: Bert pre-training of image transformers, 2022. URL https://arxiv.org/abs/2106.08254.

[3] Brian R. Bartoldson, James Diffenderfer, Konstantinos Parasyris, and Bhavya Kailkhura. Adversarial robustness limits via scaling-law and human-alignment studies, 2024. URL https://arxiv.org/abs/2404.09349.

[4] Lucas Beyer, Andreas Steiner, André Susano Pinto, Alexander Kolesnikov, Xiao Wang, Daniel Salz, Maxim Neumann, Ibrahim Alabdulmohsin, Michael Tschannen, Emanuele Bugliarello, Thomas Unterthiner, Daniel Keysers, Skanda Koppula, Fangyu Liu, Adam Grycner, Alexey Gritsenko, Neil Houlsby, Manoj Kumar, Keran Rong, Julian Eisenschlos, Rishabh Kabra, Matthias Bauer, Matko Bošnjak, Xi Chen, Matthias Minderer, Paul Voigtlaender, Ioana Bica, Ivana Balazevic, Joan Puigcerver, Pinelopi Papalampidi, Olivier Henaff, Xi Xiong, Radu Soricut, Jeremiah Harmsen, and Xiaohua Zhai. Paligemma: A versatile 3b vlm for transfer, 2024. URL https://arxiv.org/abs/2407.07726.

[5] Battista Biggio, Igino Corona, Davide Maiorca, Blaine Nelson, Nedim Srndic, Pavel Laskov, Giorgio Giacinto, and Fabio Roli. Evasion attacks against machine learning at test time. *CoRR*, abs/1708.06131, 2017. URL http://arxiv.org/abs/1708.06131.

[6] Nicolas Carion, Francisco Massa, Gabriel Synnaeve, Nicolas Usunier, Alexander Kirillov, and Sergey Zagoruyko. End-to-end object detection with transformers. *CoRR*, abs/2005.12872, 2020. URL https://arxiv.org/abs/2005.12872.

[7] Mathilde Caron, Hugo Touvron, Ishan Misra, Hervé Jégou, Julien Mairal, Piotr Bojanowski, and Armand Joulin. Emerging properties in self-supervised vision transformers. *CoRR*, abs/2104.14294, 2021. URL https://arxiv.org/abs/2104.14294.

[8] Cheng Chen, Yuhong Wang, Nafis S Munir, Xiangwei Zhou, and Xugui Zhou. Revisiting adversarial perception attacks and defense methods on autonomous driving systems, 2025. URL https://arxiv.org/abs/2505.11532.

[9] Cherti, Mehdi, Beaumont, Romain, Wightman, Ross, Wortsman, Mitchell, Ilharco, Gabriel, Gordon, Cade, Schuhmann, Christoph, Schmidt, Ludwig, Jitsev, and Jenia. Reproducible scaling laws for contrastive language-image learning. In *2023 IEEE/CVF Conference on Computer Vision and Pattern Recognition (CVPR)*, page 2818–2829. IEEE, June 2023. doi: 10.1109/cvpr52729.2023.00276. URL http://dx.doi.org/10.1109/CVPR52729.2023.00276.

[10] Francesco Croce and Matthias Hein. Reliable evaluation of adversarial robustness with an ensemble of diverse parameter-free attacks, 2020. URL https://arxiv.org/abs/2003.01690.

[11] Francesco Croce, Maksym Andriushchenko, Vikash Sehwag, Edoardo Debenedetti, Nicolas Flammarion, Mung Chiang, Prateek Mittal, and Matthias Hein. Robustbench: a standardized adversarial robustness benchmark, 2021. URL https://arxiv.org/abs/2010.09670.

[12] Gavin Weiguang Ding, Kry Yik Chau Lui, Xiaomeng Jin, Luyu Wang, and Ruitong Huang. On the sensitivity of adversarial robustness to input data distributions, 2019. URL https://arxiv.org/abs/1902.08336.

[13] Yinpeng Dong, Qi-An Fu, Xiao Yang, Tianyu Pang, Hang Su, Zihao Xiao, and Jun Zhu. Benchmarking adversarial robustness. *CoRR*, abs/1912.11852, 2019. URL http://arxiv.org/abs/1912.11852.

[14] Alexey Dosovitskiy, Lucas Beyer, Alexander Kolesnikov, Dirk Weissenborn, Xiaohua Zhai, Thomas Unterthiner, Mostafa Dehghani, Matthias Minderer, Georg Heigold, Sylvain Gelly, Jakob Uszkoreit, and Neil Houlsby. An image is worth 16x16 words: Transformers for image recognition at scale, 2021. URL https://arxiv.org/abs/2010.11929.

[15] Logan Engstrom, Brandon Tran, Dimitris Tsipras, Ludwig Schmidt, and Aleksander Madry. Exploring the landscape of spatial robustness, 2019. URL https://arxiv.org/abs/1712.02779.

[16] Alex Fang, Albin Madappally Jose, Amit Jain, Ludwig Schmidt, Alexander Toshev, and Vaishaal Shankar. Data filtering networks, 2023. URL https://arxiv.org/abs/2309.17425.

[17] Ian J. Goodfellow, Jonathon Shlens, and Christian Szegedy. Explaining and harnessing adversarial examples, 2015. URL https://arxiv.org/abs/1412.6572.

[18] Kathrin Grosse, Nicolas Papernot, Praveen Manoharan, Michael Backes, and Patrick McDaniel. Adversarial perturbations against deep neural networks for malware classification, 2016. URL https://arxiv.org/abs/1606.04435.

[19] Kaiming He, Xiangyu Zhang, Shaoqing Ren, and Jian Sun. Deep residual learning for image recognition, 2015. URL https://arxiv.org/abs/1512.03385.

[20] Kaiming He, Xiangyu Zhang, Shaoqing Ren, and Jian Sun. Deep Residual Learning for Image Recognition. In *2016 IEEE Conference on Computer Vision and Pattern Recognition (CVPR)*, pages 770–778, Las Vegas, NV, USA, June 2016. IEEE. ISBN 978-1-4673-8851-1. doi: 10.1109/CVPR.2016.90.

[21] Kaiming He, Xinlei Chen, Saining Xie, Yanghao Li, Piotr Dollár, and Ross B. Girshick. Masked autoencoders are scalable vision learners. *CoRR*, abs/2111.06377, 2021. URL https://arxiv.org/abs/2111.06377.

[22] Dan Hendrycks and Thomas Dietterich. Benchmarking neural network robustness to common corruptions and perturbations, 2019. URL https://arxiv.org/abs/1903.12261.

[23] Dan Hendrycks, Steven Basart, Norman Mu, Saurav Kadavath, Frank Wang, Evan Dorundo, Rahul Desai, Tyler Zhu, Samyak Parajuli, Mike Guo, Dawn Song, Jacob Steinhardt, and Justin Gilmer. The many faces of robustness: A critical analysis of out-of-distribution generalization, 2021. URL https://arxiv.org/abs/2006.16241.

[24] Martin Heusel, Hubert Ramsauer, Thomas Unterthiner, Bernhard Nessler, Günter Klambauer, and Sepp Hochreiter. Gans trained by a two time-scale update rule converge to a nash equilibrium. *CoRR*, abs/1706.08500, 2017. URL http://arxiv.org/abs/1706.08500.

[25] Hossein Hosseini and Radha Poovendran. Semantic adversarial examples, 2018. URL https://arxiv.org/abs/1804.00499.

[26] Jeremy Howard. Imagenette: A smaller subset of imagenet for rapid prototyping. https://github.com/fastai/imagenette, 2019. Accessed: 2025-08-01.

[27] Nikolaus Howe, Ian McKenzie, Oskar Hollinsworth, Michał Zajac, Tom Tseng, Aaron Tucker, Pierre-Luc Bacon, and Adam Gleave. Scaling trends in language model robustness, 2025. URL https://arxiv.org/abs/2407.18213.

[28] Lei Hsiung, Yun-Yun Tsai, Pin-Yu Chen, and Tsung-Yi Ho. Towards compositional adversarial robustness: Generalizing adversarial training to composite semantic perturbations, 2023. URL https://arxiv.org/abs/2202.04235.

[29] Yahya Jabary. Self-ensembling. https://github.com/ETH-DISCO/self-ensembling, 2024. Accessed: 2025-07-30.

[30] Yahya Jabary, Andreas Plesner, Turlan Kuzhagaliyev, and Roger Wattenhofer. Seeing through the mask: Rethinking adversarial examples for captchas, 2024. URL https://arxiv.org/abs/2409.05558.

[31] Alex Krizhevsky, Ilya Sutskever, and Geoffrey E Hinton. ImageNet Classification with Deep Convolutional Neural Networks. In *Advances in Neural Information Processing Systems*, volume 25. Curran Associates, Inc., 2012.

[32] Yann LeCun, Yoshua Bengio, and Geoffrey Hinton. Deep learning. *Nature*, 521(7553):436–444, 2015. doi: 10.1038/nature14539. URL https://doi.org/10.1038/nature14539.

[33] Ze Liu, Yutong Lin, Yue Cao, Han Hu, Yixuan Wei, Zheng Zhang, Stephen Lin, and Baining Guo. Swin transformer: Hierarchical vision transformer using shifted windows, 2021. URL https://arxiv.org/abs/2103.14030.

[34] Ze Liu, Han Hu, Yutong Lin, Zhuliang Yao, Zhenda Xie, Yixuan Wei, Jia Ning, Yue Cao, Zheng Zhang, Li Dong, Furu Wei, and Baining Guo. Swin transformer v2: Scaling up capacity and resolution, 2022. URL https://arxiv.org/abs/2111.09883.

[35] Zhuang Liu, Hanzi Mao, Chao-Yuan Wu, Christoph Feichtenhofer, Trevor Darrell, and Saining Xie. A convnet for the 2020s, 2022. URL https://arxiv.org/abs/2201.03545.

[36] Aleksander Madry, Aleksandar Makelov, Ludwig Schmidt, Dimitris Tsipras, and Adrian Vladu. Towards deep learning models resistant to adversarial attacks, 2019. URL https://arxiv.org/abs/1706.06083.

[37] Maxime Oquab, Timothée Darcet, Théo Moutakanni, Huy Vo, Marc Szafraniec, Vasil Khalidov, Pierre Fernandez, Daniel Haziza, Francisco Massa, Alaaeldin El-Nouby, Mahmoud Assran, Nicolas Ballas, Wojciech Galuba, Russell Howes, Po-Yao Huang, Shang-Wen Li, Ishan Misra, Michael Rabbat, Vasu Sharma, Gabriel Synnaeve, Hu Xu, Hervé Jegou, Julien Mairal, Patrick Labatut, Armand Joulin, and Piotr Bojanowski. Dinov2: Learning robust visual features without supervision, 2024. URL https://arxiv.org/abs/2304.07193.

[38] Nicolas Papernot, Patrick McDaniel, Ian Goodfellow, Somesh Jha, Z. Berkay Celik, and Ananthram Swami. Practical black-box attacks against machine learning, 2017. URL https://arxiv.org/abs/1602.02697.

[39] Zhiliang Peng, Li Dong, Hangbo Bao, Qixiang Ye, and Furu Wei. Beit v2: Masked image modeling with vector-quantized visual tokenizers, 2022. URL https://arxiv.org/abs/2208.06366.

[40] Andreas Plesner, Tobias Vontobel, and Roger Wattenhofer. Breaking recaptchav2. In *2024 IEEE 48th Annual Computers, Software, and Applications Conference (COMPSAC)*, pages 1047–1056. IEEE, 2024.

[41] Alec Radford, Jong Wook Kim, Chris Hallacy, Aditya Ramesh, Gabriel Goh, Sandhini Agarwal, Girish Sastry, Amanda Askell, Pamela Mishkin, Jack Clark, Gretchen Krueger, and Ilya Sutskever. Learning transferable visual models from natural language supervision. *CoRR*, abs/2103.00020, 2021. URL https://arxiv.org/abs/2103.00020.

[42] Sylvestre-Alvise Rebuffi, Sven Gowal, Dan A. Calian, Florian Stimberg, Olivia Wiles, and Timothy Mann. Fixing data augmentation to improve adversarial robustness, 2021. URL https://arxiv.org/abs/2103.01946.

[43] Edgar Riba, Dmytro Mishkin, Daniel Ponsa, Ethan Rublee, and Gary Bradski. Kornia: an open source differentiable computer vision library for pytorch, 2019. URL https://arxiv.org/abs/1910.02190.

[44] Olaf Ronneberger, Philipp Fischer, and Thomas Brox. U-Net: Convolutional Networks for Biomedical Image Segmentation. In Nassir Navab, Joachim Hornegger, William M. Wells, and Alejandro F. Frangi, editors, *Medical Image Computing and Computer-Assisted Intervention – MICCAI 2015*, pages 234–241, Cham, 2015. Springer International Publishing. ISBN 978-3-319-24574-4. doi: 10.1007/978-3-319-24574-4_28.

[45] Olga Russakovsky, Jia Deng, Hao Su, Jonathan Krause, Sanjeev Satheesh, Sean Ma, Zhiheng Huang, Andrej Karpathy, Aditya Khosla, Michael Bernstein, Alexander C. Berg, and Li Fei-Fei. Imagenet large scale visual recognition challenge, 2015. URL https://arxiv.org/abs/1409.0575.

[46] Andrew Seong. Exploring the vulnerability of the state-of-the-art content moderation image classifiers against adversarial attacks. Master's thesis, The University of Texas at San Antonio, San Antonio, TX, USA, December 2023. URL https://rrpress.utsa.edu/server/api/core/bitstreams/239196ef-e3b9-4692-ba49-ec911c413811/content. Accessed: 2025-08-10.

[47] Naman D Singh, Francesco Croce, and Matthias Hein. Revisiting adversarial training for imagenet: Architectures, training and generalization across threat models, 2023. URL https://arxiv.org/abs/2303.01870.

[48] Christian Szegedy, Wojciech Zaremba, Ilya Sutskever, Joan Bruna, Dumitru Erhan, Ian Goodfellow, and Rob Fergus. Intriguing properties of neural networks, 2014. URL https://arxiv.org/abs/1312.6199.

[49] Michael Tschannen, Alexey Gritsenko, Xiao Wang, Muhammad Ferjad Naeem, Ibrahim Alabdulmohsin, Nikhil Parthasarathy, Talfan Evans, Lucas Beyer, Ye Xia, Basil Mustafa, Olivier Hénaff, Jeremiah Harmsen, Andreas Steiner, and Xiaohua Zhai. Siglip 2: Multilingual vision-language encoders with improved semantic understanding, localization, and dense features, 2025. URL https://arxiv.org/abs/2502.14786.

[50] Ultralytics. Ultralytics github repository. https://github.com/ultralytics/ultralytics, 2025. Accessed: 2025-08-05.

[51] Xiaohua Zhai, Basil Mustafa, Alexander Kolesnikov, and Lucas Beyer. Sigmoid loss for language image pre-training, 2023. URL https://arxiv.org/abs/2303.15343.

A Model Specifications of the Robustness Scaling Analysis

B Attacks

As mentioned in the main text, we consider a black-box threat model in which adversaries have no access to the model's architecture, parameters, or gradients [38], and we impose no constraints on the perturbation magnitude, enabling exploration of a broader range of attack strategies. Appendix C contains additional sample images.

B.1 Random Perturbations

The Random Perturbations comprise four distinct perturbation variants, each targeting a specific image property: hue, saturation, contrast, or brightness. These attacks modify their respective properties within predefined bounds through uniform random sampling for each image. The attacks are implemented as dynamic transformations integrated directly into the model's preprocessing pipeline using the Python library Kornia [43]. The perturbations are applied before any standard preprocessing operations, ensuring that the model encounters perturbed inputs without any prior adaptation. Each variant operates independently and was applied to the entire ImageNet validation split.

B.2 GeometricMasksV1

The GeometricMasksV1 attack employs HCaptcha-inspired geometric overlays to evaluate model robustness against structured occlusions [30]. This attack category comprises four distinct mask patterns, namely Circle, Diamond, Square, and Knit, each designed to systematically obscure portions of the input image while preserving overall semantic interpretability. We applied the Circle mask to the entire ImageNet validation set at four opacity levels: $\alpha \in \{50, 80, 110, 140\}$, where α represents the opacity value on a 0-255 scale.

B.3 GeometricMasksV2

GeometricMasksV2 extends the functionality of GeometricMasksV1 by enabling more flexible parametrization of mask configurations [29]. The naming convention follows a systematic format:

Table 2: Models used in the Robustness Scaling Analysis. IN1k = ImageNet-1K, IN21k = ImageNet-21K. A bracket following the dataset name (e.g., LAION-2B(1.6B)) indicates the size of the subset (1.6B images) used during training.

Model Name	Training Dataset	Training Procedure	Num. Parameters (M)	Training Data Size (M)
ResNet50	IN1k	supervised	25.6	1.2
ViT-B-16-224	IN21k+IN1k	supervised	88.3	14.0
ViT-B-32-384	IN21k+IN1k	supervised	88.3	14.0
ViT-L-16-384	IN21k+IN1k	supervised	306.7	14.0
ViT-L-32-384	IN21k+IN1k	supervised	306.7	14.0
CLIP-VIT-B-16	DFN-2B	contrastive	149.6	2000.0
CLIP-VIT-B-32-QuickGELU	OPENAI-WIT	contrastive	151.3	400.0
CLIP-VIT-B-32-QuickGELU	LAION-400M	contrastive	151.3	413.0
CLIP-VIT-B-32	LAION-2B	contrastive	151.3	2000.0
CLIP-EVA02-B-16	LAION-2B(1.6B) + COYO-700M(400M)	contrastive	149.6	2000.0
CLIP-VIT-L-14-QuickGELU	MetaClip400M	contrastive	427.6	400.0
CLIP-VIT-L-14-QuickGELU	OPENAI-WIT	contrastive	427.6	400.0
CLIP-VIT-L-14	DataComp-1B	contrastive	427.6	1400.0
CLIP-VIT-L-14	MetaClip full CC	contrastive	427.6	2500.0
CLIP-VIT-L-14	DFN-2B	contrastive	427.6	2000.0
CLIP-EVA02-L-14	LAION-2B(1.6B) + COYO-700M(400M)	contrastive	427.6	2000.0
CLIP-VIT-H-14	DFN-5B	contrastive	986.1	5000.0
DINOv2-S	LVD-142M	self-supervised	22.8	142.0
DINOv2-B	LVD-142M	self-supervised	86.6	142.0
DINOv2-L	LVD-142M	self-supervised	306.0	142.0
DINOv2-G	LVD-142M	self-supervised	1140.0	142.0
SWIN-L-384	IN1k	supervised	197.0	1.2
SWINv2-L-384	IN21k+IN1k	supervised	198.0	14.0
ConvNext-L	IN21k+IN1k	supervised	198.0	14.0
YOLO11m-cls	IN1k	supervised	20.0	1.2
ViT-MAE	IN1k	self-supervised	112.0	1.2
DINOv1-ViT-B-16	IN1k	self-supervised	86.9	1.2
PaliGemma3b	many	self-supervised	2920.0	22256.0
BEIT-B-16-224	IN21k+IN1k	self-supervised	86.0	14.0
BEIT-L-16-224	IN21k+IN1k	self-supervised	307.0	14.0
BEITv2-B-16-224-1K-1K	IN1k+IN1k	self-supervised	86.0	1.2
BEITv2-B-16-224-22K-1K	IN1k+(IN21k+IN1k)	self-supervised	86.0	14.0
SIGLIP-SO400-14-384	WebLI	contrastive	878.0	22000.0
SIGLIP2-SO400-14-384	WebLI	contrastive	1136.0	22000.0
SIGLIP-B-16-224	WebLI	contrastive	203.0	22000.0
SIGLIP2-B-16-224	WebLI	contrastive	375.0	22000.0

Table 3: Fine-tuning configurations for pre-trained models on ImageNet.

Model	**Epochs**	**LR**	**Batch Size**	**Weight Decay**	**Optimizer**
ViT-MAE	10	3×10^{-4}	32	–	AdamW
DINOv1	5	1×10^{-3}	128	–	AdamW
PaliGemma	1	1×10^{-3}	64	0.01	AdamW

[number of sides per polygon]-[number of polygons per row and column]-[number of concentric polygons] [color scheme]. This approach generates diverse geometric occlusion patterns that preserve semantic content while introducing systematic visual perturbations. Each mask variant was applied to the complete ImageNet validation set.

B.4 Coco Objects

In the Coco Objects attack, we employed Facebook's DETR object detection model with a Resnet50 backbone to crop subject objects from the ImageNet validation split [6]. Each cropped result underwent manual review, with outcomes systematically recorded in CSV files organized by class for later reuse. Manual evaluation of 120 classes yielded 3378 images with correct cropping. Images

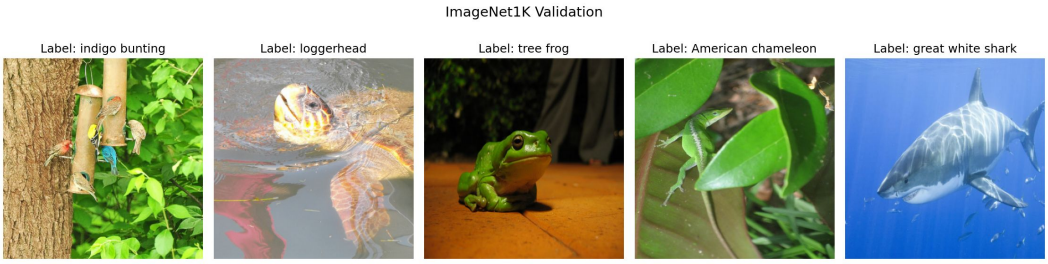

Figure 6: Sample images from the clean ImageNet1k validation split

Figure 7: Sample images from the Random Perturbations attack

where the cropped mask occupied less than 1% or more than 60% of the original image area were subsequently filtered, resulting in a final dataset of 2055 images. The cropped subjects were then composited onto three background types: solid black, thresholded Perlin noise based on Yahya Jabary's implementation [29], and continuous Perlin noise, while preserving the original size and spatial positioning of the cropped elements. Attack success rates were computed using the unmodified original versions of the 2055 selected images as the baseline reference.

B.5 ImageNet-C

ImageNet-C comprises 19 distinct perturbations categorized into noise, blur, weather, and digital corruption types [22]. Each corruption was systematically applied to the complete ImageNet validation split across five graduated severity levels, where severity 1 represents the lightest perturbation and severity 5 constitutes the most vigorous corruption intensity. The experimental protocol evaluated model performance at each severity level using randomly sampled subsets of 100,000 images drawn from across all 19 distinct perturbations to ensure computational feasibility while maintaining statistical validity.

B.6 ImageNet-R

ImageNet-R consists of a 200-class subset derived from ImageNet, featuring a test set of 30,000 images that contain diverse artistic and stylistic renditions of standard object categories [23]. These renditions encompass various non-photographic representations, including paintings, embroidery, sketches, and other artistic interpretations, challenging model robustness to domain shift and stylistic variation while maintaining semantic content consistency with the original ImageNet classification task. As no direct clean counterparts exist for these artistic renditions, the attack success rate was approximated using ImageNet-200, the corresponding 200-class subset of the ImageNet validation dataset, as the clean baseline for measuring accuracy degradation [23]. Since ImageNet-R contains only 200 of the original 1000 ImageNet classes, model predictions for ImageNet-R and ImageNet-200 were restricted to these 200 classes.

C Sample Images of the Attacks Employed in the Robustness Analysis

The Random Perturbation attacks were applied as follows:

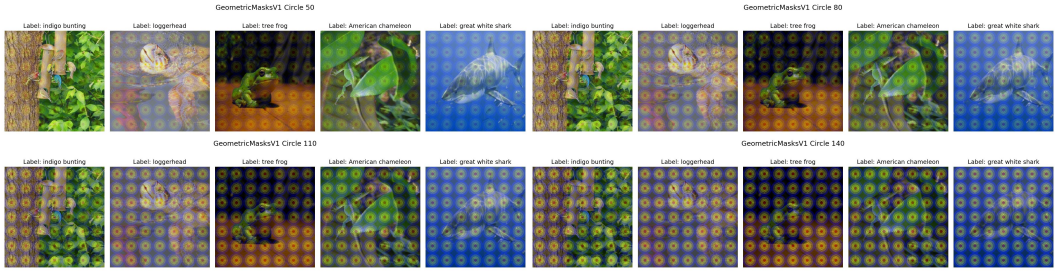

Figure 8: Sample images from the GeometricMasksV1 attack

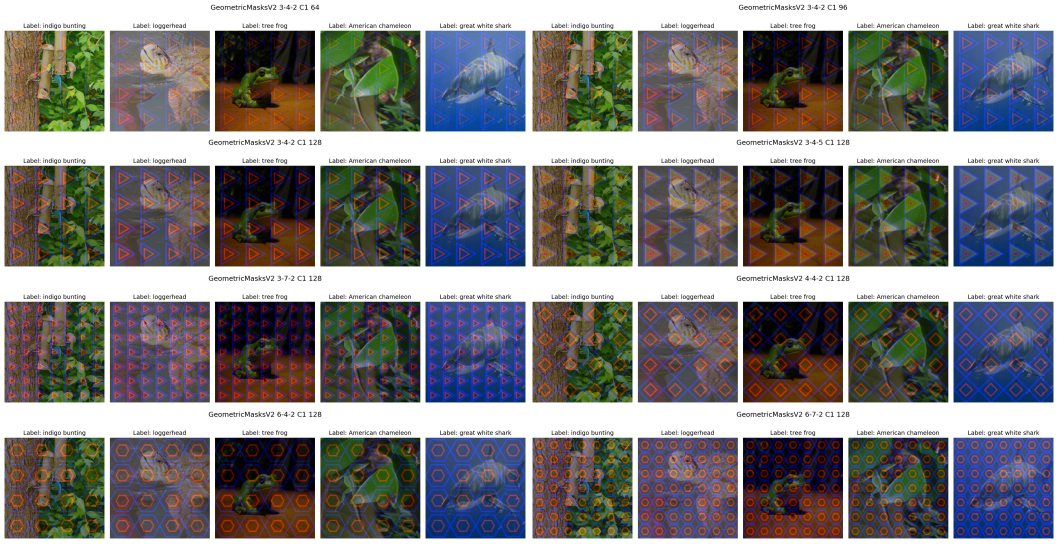

Figure 9: Sample images from the GeometricMasksV2 attack

- **Hue perturbation** ($\delta_h = 0.5$): Applies a random hue shift $h \sim \mathcal{U}(-0.5, 0.5)$ in HSV colour space, where values represent fractions of the full hue rotation cycle.

- **Saturation perturbation** ($\delta_s = 0.9$): Multiplies pixel saturation by a factor $s \sim \mathcal{U}(0.1, 1.9)$, enabling transitions from near-grayscale ($s = 0.1$) to highly saturated ($s = 1.9$) conditions.

- **Contrast perturbation** ($\delta_c = 0.9$): Adjusts image contrast through scaling pixel intensities $I' = I \times c$, where $c \sim \mathcal{U}(0.1, 1.9)$.

- **Brightness perturbation** ($\delta_b = 0.7$): Shifts pixel intensities $I' = I + b$ by a factor $b \sim \mathcal{U}(0.3, 1.7)$, uniformly modulating image luminance across all channels.

D Sample Images of the Adversarial Fine-Tuning Evaluation

The random mask in the fine-tuning of ResNet50-v3 was randomly chosen for each perturbed image from the configurations *[3, 4, 6, 10]-[2, 4, 7, 10]-[2, 5, 10] [C1, C2]* as shown in Figures 13 and 14.

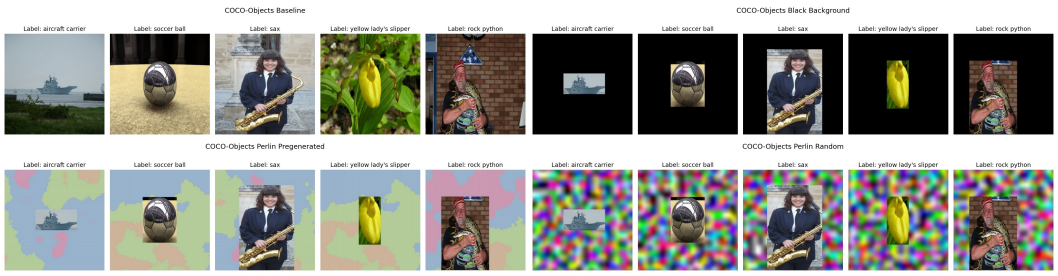

Figure 10: Sample images from the COCO Objects attack

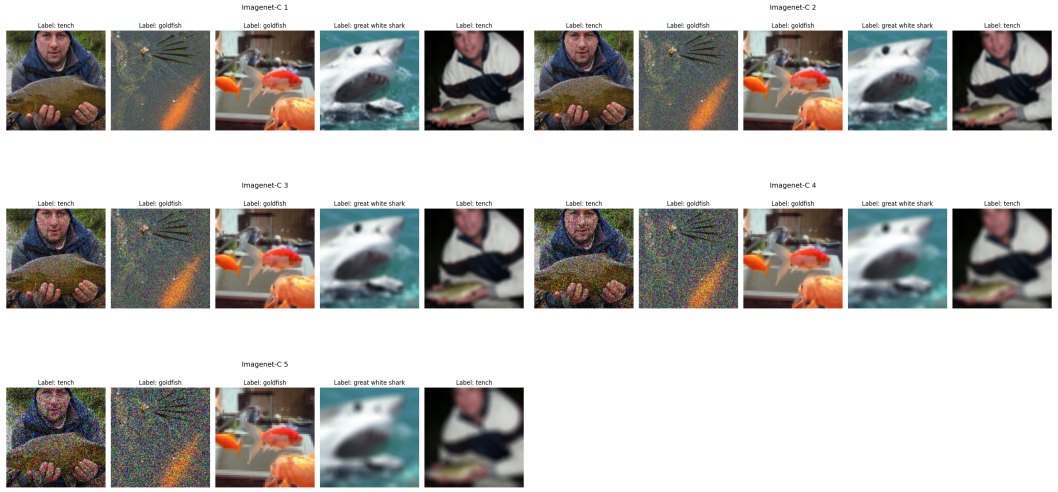

Figure 11: Sample images from the five severity levels in ImageNet-C

E Human Evaluation GUI

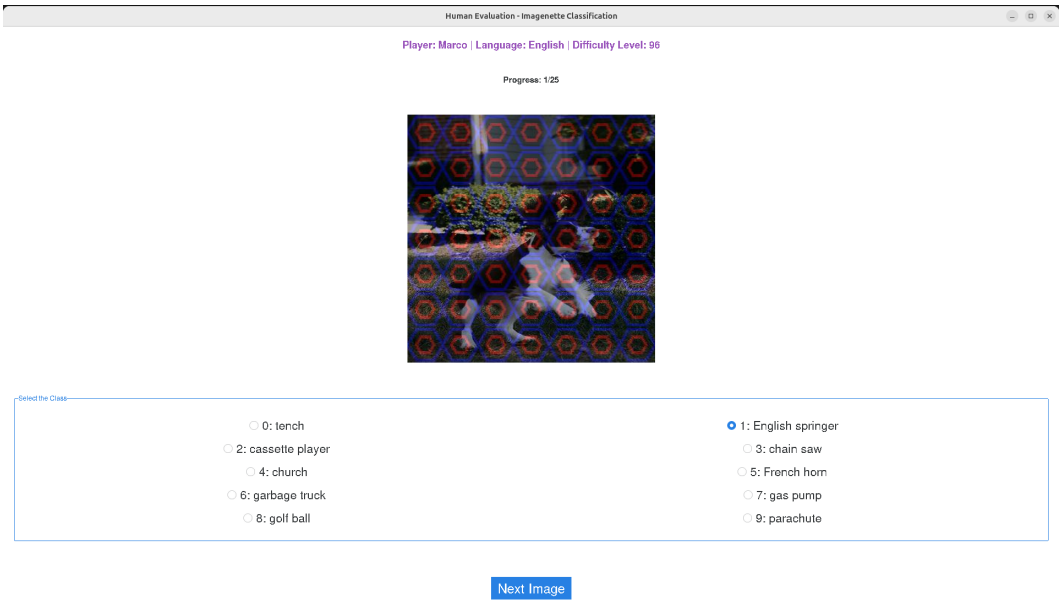

Figure 15: Graphical user interface (GUI) used for the human evaluation task

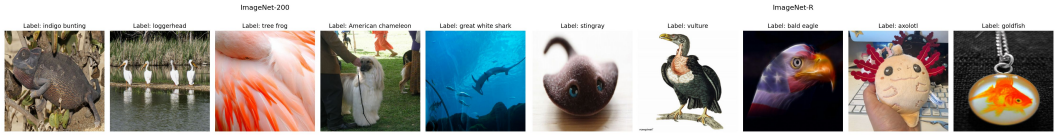

Figure 12: Sample images from ImageNet-200 and ImageNet-R

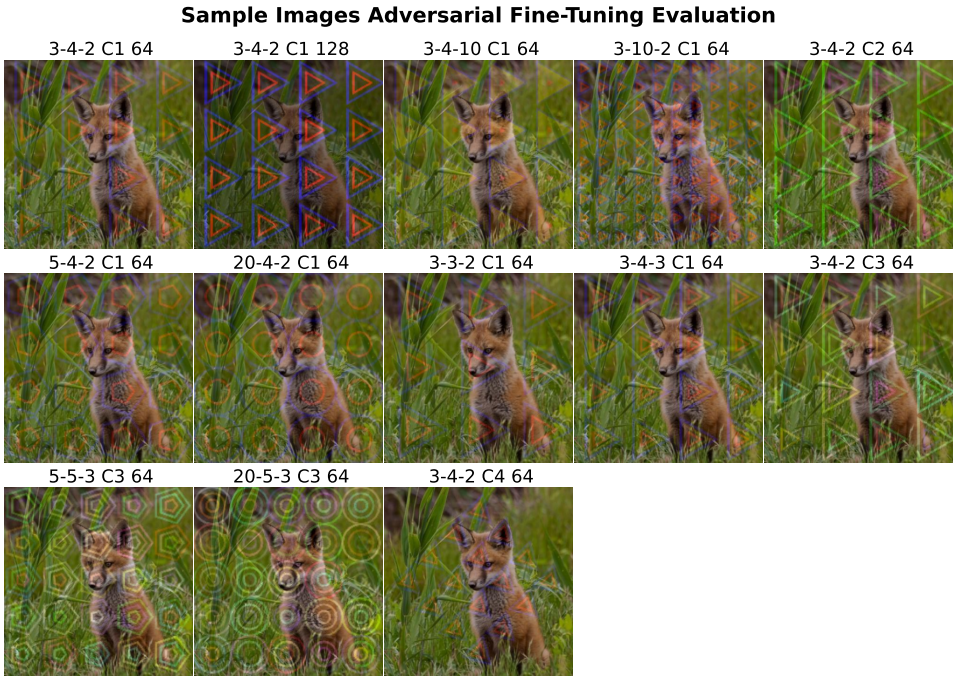

Figure 13: Sample images of the GeometricMasksV2 configurations used in the evaluation of the adversarially fine-tuned ResNet50s

F Comparisons of Models

F.1 Comparison of CLIP models

Table 4: Attack success rates (%) for selected CLIP-ViT-L-14 models

Attack Category	Attack Type	VIT-L-14- METACLIP 400M	VIT-L-14 METACLIP FULLCC	APPLE DFN2B-CLIP-VIT-L-14	EVA02-L-14
Random	Hue 0.5	16.1	14.5	10.8	11.5
	Saturation 0.9	4.1	3.5	2.2	2.3
	Contrast 0.9	6.1	5.3	3.1	3.5
	Brightness 0.7	15.0	13.8	9.7	8.7
GeometricMasksV1	Circle 50	23.2	18.8	15.0	11.6
	Circle 80	43.2	35.3	35.5	24.9
	Circle 110	63.8	55.6	63.2	44.9
	Circle 140	83.0	77.3	87.7	69.8
GeometricMasksV2	3-4-2 C1 Opacity 64	17.2	14.1	11.2	10.1
	3-4-2 C1 Opacity 96	22.7	19.6	18.4	15.2
	3-4-2 C1 Opacity 128	28.8	25.8	27.3	21.8
	3-4-5 C1 Opacity 128	30.8	26.8	28.4	22.3
	3-7-2 C1 Opacity 128	43.1	37.0	47.5	34.2
	6-4-2 C1 Opacity 128	48.8	51.3	53.2	42.4
	6-7-2 C1 Opacity 128	69.0	72.7	79.0	62.2
COCO Objects	Black Background	20.5	19.0	16.4	13.6
	Thresholded Perlin Noise Background	22.0	21.0	17.9	15.8
	Perlin Noise Background	27.5	24.0	21.4	17.2
ImageNet-R	ImageNet-R	9.5	8.3	9.0	6.3
ImageNet-C	Distortion Severity 1	10.4	8.5	6.7	5.4
	Distortion Severity 2	18.7	16.1	13.5	9.4
	Distortion Severity 3	25.8	22.0	19.3	13.2
	Distortion Severity 4	37.9	32.4	28.7	19.4
	Distortion Severity 5	51.6	45.5	41.6	29.6
Overall Average	Mean of Averages per Attack Category	27.1	24.3	24.0	18.5

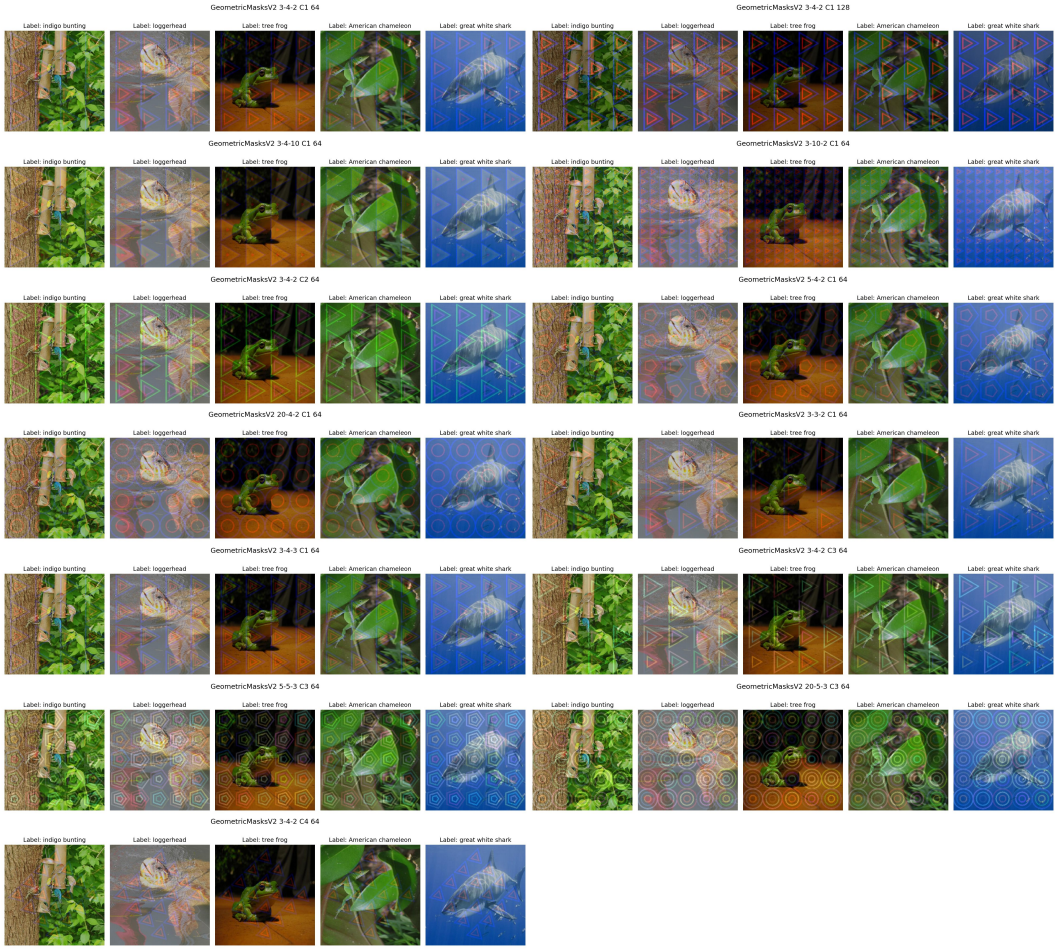

Figure 14: Sample images from the GeometricMasksV2 attack used for the ResNet50 fine-tuning and validation

Four CLIP-ViT-L-14 variants with identical architectures but distinct training datasets reveal attack-specific vulnerability patterns that illuminate the relationship between data curation strategies and robustness mechanisms in Table 4.

Random Perturbations expose fundamental differences in color invariance learning. EVA02-L-14 and DFN-2B demonstrate superior resilience, while MetaClip variants show almost doubled vulnerability. The stark contrast in hue and brightness perturbation resistance suggests that multi-source curation (LAION-2B + COYO-700M) and quality filtering (DFN-2B) better preserve color and brightness consistency during training than metadata-based selection alone.

In the GeometricMasksV1 category, EVA02-L-14 maintains a significant advantage, and MetaCLIP FullCC consistently outperforms the 400M version. DFN-2B unexpectedly deteriorates increasingly, starting at occlusion 80, exceeding even MetaClip-400M. This vulnerability inversion indicates that DFN-2B's quality filtering may systematically exclude partially occluded objects, creating blind spots that manifest under severe geometric perturbations.

GeometricMasksV2 attacks demonstrate complex pattern-dependent vulnerabilities. EVA02-L-14 maintains the lowest attack success rates with an advantage of more than 10%. DFN-2B again shows deteriorated performance on opacities above 96. The MetaCLIP models perform similarly to DFN-2B, but surprisingly, the masks 6-4-2 C1 and 6-7-2 C2 invert the ordering of the MetaCLIP models' performance, with the 400M version outperforming the FullCC one.

COCO Objects manipulations show relatively compressed performance differences (13.6-27% ASR range). EVA02-L-14 performs the best, with DFN-2B having an ASR increased by about 2-3%. The

MetaCLIP models show an even higher vulnerability. While the MetaCLIP FullCC outperforms the 400M version, it has an ASR which is between 32% and 39% higher than that of EVA02-L-14.

ImageNet-R produces the tightest clustering of results (6.3-9.5% ASR), suggesting that artistic domain shifts probe fundamental visual representations largely independent of training data characteristics. However, one has to keep in mind that all four models have been trained on relatively large datasets. The minimal variation indicates that current CLIP training strategies, regardless of scale or curation method, develop similar capabilities for handling stylistic variations.

ImageNet-C corruptions reveal progressive differentiation with severity. At low severities, performance differences remain modest (at most 5% at severity 1), but diverge substantially at maximum corruption (29.6-51.6% at severity 5, a relative increase of up to 74%). EVA02-L-14's consistent advantage across all severity levels—maintaining sub-30% ASR even at severity 5—demonstrates that combining high-quality datasets from multiple sources builds more robust representations against naturalistic corruptions than single-source approaches.

These attack-specific patterns establish that training data characteristics influence robustness mechanisms differentially across perturbation types. Multi-source curation (EVA02-L-14) provides consistent advantages across all attack categories, while quality-focused filtering (DFN-2B) creates asymmetric robustness profiles with specific vulnerabilities to geometric occlusions. Scale without quality control (MetaClip Full CC) offers minimal benefits, indicating that strategic data curation supersedes volume for comprehensive adversarial robustness.

F.2 Comparison of BEiTv2 Models

Table 5: Attack success rates (%) for selected BEiTv2 models

Attack Category	Attack Type	BEITV2 B 16 224 IN1K FT IN1K	BEITV2 B 16 224 IN1K FT IN22K IN1K
Random	Hue 0.5	7.7	7.9
	Saturation 0.9	1.2	1.1
	Contrast 0.9	1.5	1.3
	Brightness 0.7	5.8	5.5
GeometricMasksV1	Circle 50	11.0	7.0
	Circle 80	19.7	11.5
	Circle 110	34.5	24.5
	Circle 140	58.4	54.4
GeometricMasksV2	3-4-2 C1 Opacity 64	8.8	5.7
	3-4-2 C1 Opacity 96	12.9	9.4
	3-4-2 C1 Opacity 128	17.9	20.7
	3-4-5 C1 Opacity 128	19.6	18.5
	3-7-2 C1 Opacity 128	32.4	29.8
	6-4-2 C1 Opacity 128	77.9	49.9
	6-7-2 C1 Opacity 128	68.7	69.0
COCO Objects	Black Background	9.8	10.8
	Thresholded Perlin Noise Background	15.1	11.8
	Perlin Noise Background	61.1	23.9
ImageNet-R	ImageNet-R	35.2	30.8
ImageNet-C	Distortion Severity 1	7.7	6.6
	Distortion Severity 2	12.1	11.2
	Distortion Severity 3	17.4	14.5
	Distortion Severity 4	24.6	20.7
	Distortion Severity 5	36.2	31.1
Overall Average	Mean of Averages per Attack Category	25.4	20.1

The comparison between BEiTv2 Base Patch-16 models fine-tuned exclusively on ImageNet-1K versus sequential fine-tuning on ImageNet-21K followed by ImageNet-1K in Table 5 reveals consistent improvements in adversarial robustness. The extended fine-tuning protocol reduces the overall average ASR from 25.4% to 20.1%, representing a relative improvement of 20.8%.

Random color perturbations show low ASRs for both models, with the models performing almost identically, indicating that the small ImageNet-1K suffices against these low-level vulnerabilities, and expanding the dataset with ImageNet-21K does not lead to significant improvements.

Extended fine-tuning demonstrates the most substantial benefits against geometric occlusions. For GeometricMasksV1, the improvement scales with perturbation severity: minimal gains at low opacity expand up to higher occlusions of 110. The most striking improvement occurs in GeometricMasksV2 attacks, particularly for the 6-4-2 C1 configuration, where ASR decreases from 77.9% to 49.9%.

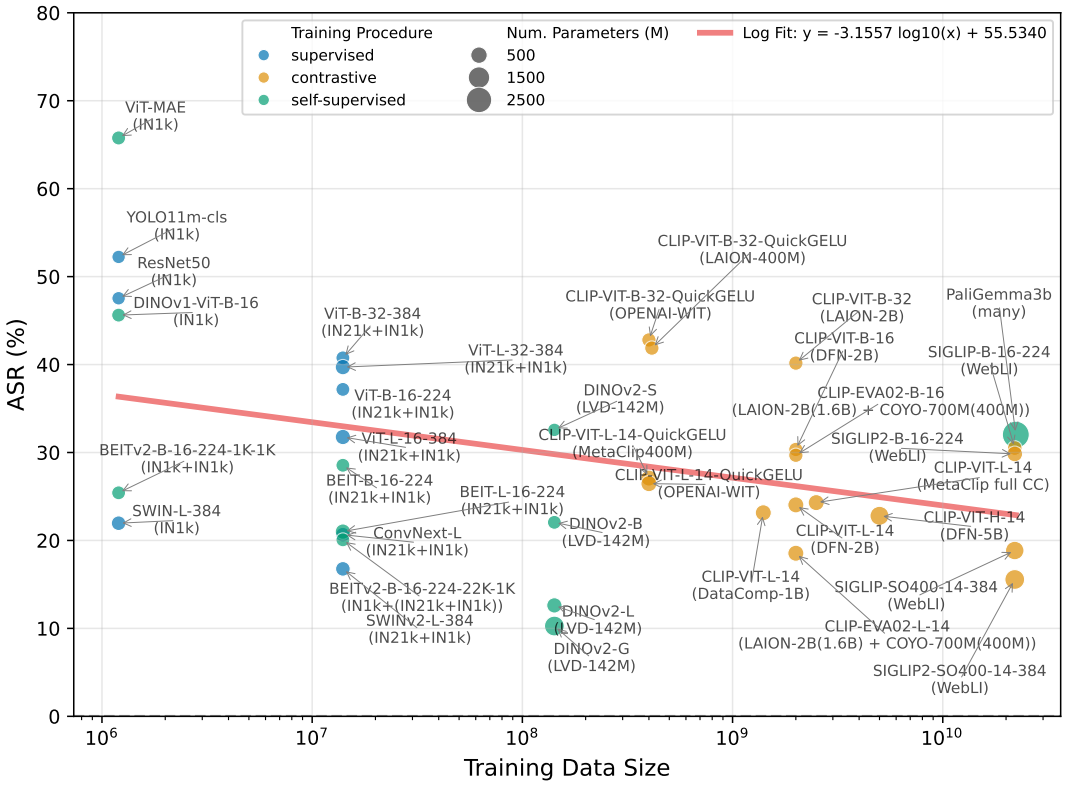

Figure 16: Overall average ASR relative to the size of the training data averaged across: Random Perturbation, GeometricMasksV1, GeometricMasksV2, Coco Objects, ImageNet-C, and ImageNet-R attacks.

However, for the other configurations in the GeometricMasksV2 category, there is little to no improvement.

Background manipulation attacks reveal selective improvements. While performance on black and thresholded Perlin backgrounds shows modest gains, the most significant reduction occurs with continuous Perlin noise backgrounds, indicating that extended fine-tuning particularly strengthens robustness to complex textural perturbations. This asymmetric improvement pattern suggests that ImageNet-21K exposure specifically addresses vulnerabilities to high-frequency noise patterns.

The benefits extend uniformly across corruption severities in ImageNet-C, with consistent relative improvements of 13-16% across all levels. Similarly, ImageNet-R shows a reduction from 35.23% to 30.78%, demonstrating that the expanded fine-tuning enhances generalization to artistic domain shifts.

These results indicate that hierarchical fine-tuning on progressively focused datasets (ImageNet-21K and ImageNet-1K) provides a more robust feature hierarchy than direct ImageNet-1K fine-tuning, particularly for spatially structured perturbations and complex backgrounds, while maintaining competitive performance on standard corruptions.

G Extra/detailed results

G.1 Overall results with labels for all points

G.2 Attack success rate per attack type

The attack success rates exhibit markedly different patterns across attack types, with the fitted logarithmic curves revealing distinct vulnerabilities in model robustness. While Random Perturbations and ImageNet-C demonstrate moderate declining trends in Figures 18a and 18e, ImageNet-R in

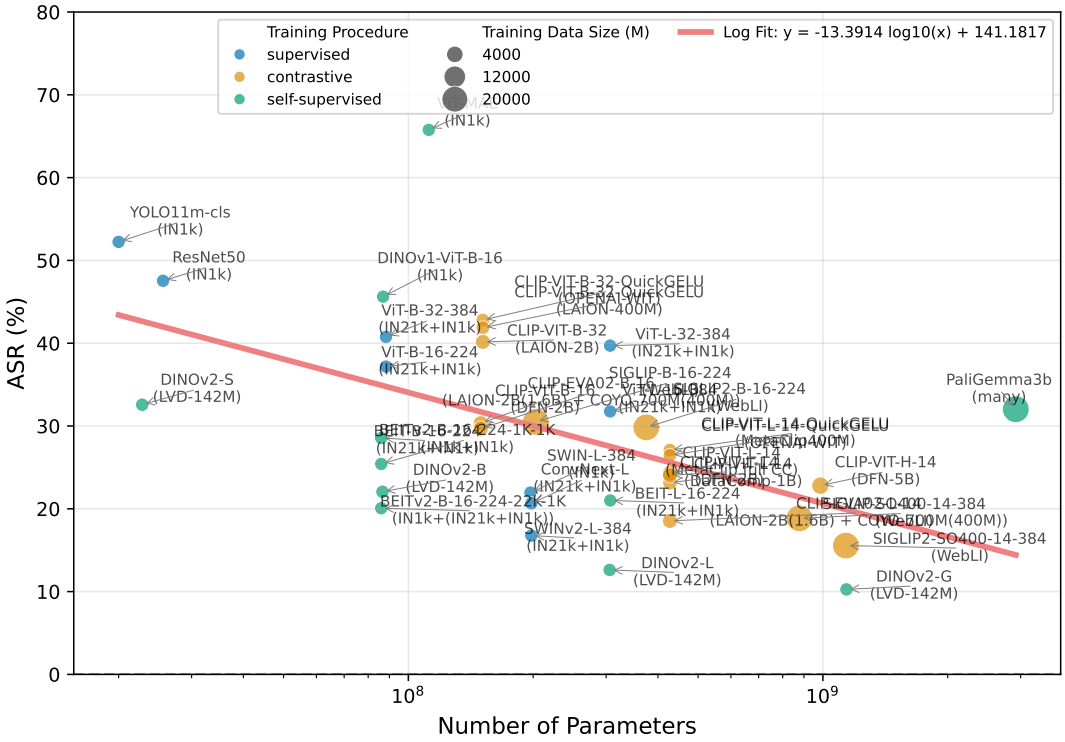

Figure 17: Overall average ASR relative to the number of model parameters averaged across: Random Perturbation, GeometricMasksV1, GeometricMasksV2, Coco Objects, ImageNet-C, and ImageNet-R attacks.

Figure 18f shows a dramatically steeper decrease, indicating that increased training data provides substantially greater protection against stylistic domain shifts than against common corruptions. This divergence likely stems from the fundamental nature of these attacks: ImageNet-C introduces perturbations such as noise, blur, and weather effects that are typically absent from standard training datasets, resulting in consistent vulnerability across models regardless of training data scale. In contrast, ImageNet-R's artistic renditions and alternative representations may be partially captured within large-scale training corpora, enabling models trained on extensive datasets to develop more robust features for handling stylistic variations. The intermediate trends observed in geometric mask attacks and COCO Objects perturbations suggest that structured occlusions and background manipulations represent a middle ground, where training data scale provides meaningful but limited improvements in robustness.

G.2.1 Training Procedure and Adversarial Robustness

Looking at Figure 19, showing the overall average attack success rates by training procedure, the relationship between training methodology and adversarial robustness appears surprisingly limited. Contrastive learning shows the lowest average ASR at 27.9%, indicating only a modest benefit from cross-modal alignment in learning robust representations. Self-supervised learning shows similar performance to contrastive learning at 28.4%, while supervised learning shows the highest vulnerability with 34.3% on average. However, the wide standard deviations reveal significant overlap across all three training paradigms, which suggests that implementation details and architectural choices may have a greater impact than the core training procedure itself.

G.3 Dataset Source and Adversarial Robustness

Figure 20 compares the scaling behavior of ASR between models trained on web-crawled and non-web-crawled datasets. For non-web-crawled datasets, the fitted relationship is ASR $= -4.3797 \log_{10}(x) + 63.1610$ while for web-crawled datasets it is ASR $= -4.4031 \log_{10}(x) + 69.9639$.

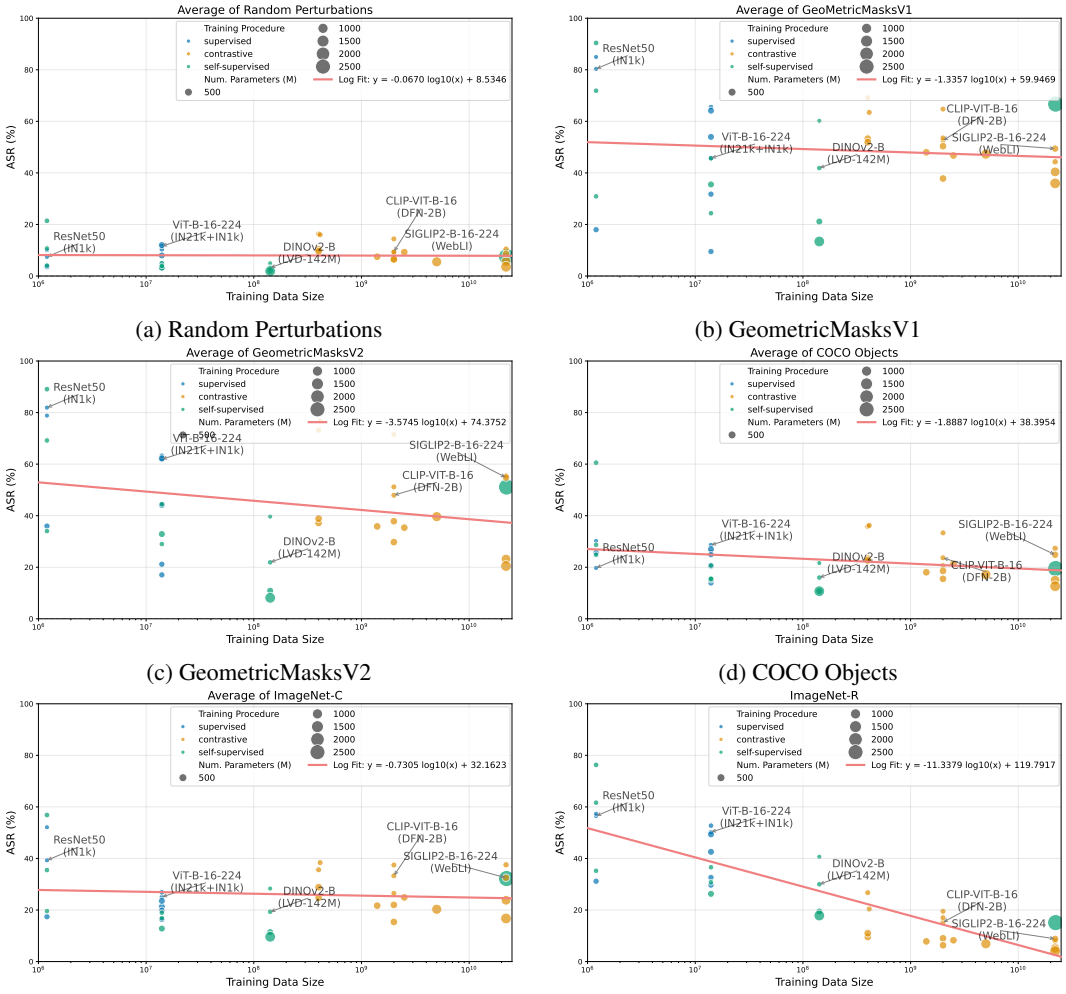

(a) Random Perturbations

(b) GeometricMasksV1

(c) GeometricMasksV2

(d) COCO Objects

(e) ImageNet-C

(f) ImageNet-R

Figure 18: Average attack success rates per attack type

At first sight, the two fitted functions appear nearly identical, differing only slightly in slope and intercept. According to this estimate, models trained on non-web-crawled datasets would require in the order of 2.63×10^{14} examples ($\approx$ 263 trillion) to achieve an ASR of zero. In contrast, models trained on web-crawled data would require roughly 7.65×10^{15} examples ($\approx$ 7.65 quadrillion). This corresponds to a factor of about $29\times$ more training data for web-crawled models to reach the same level of robustness. These results make clear that raw scale alone cannot close the robustness gap.

G.4 Worst-Case Analysis of Geometric masks

Figure 21 shows the maximum attack success rates (ASR) for the two GeometricMasks categories across a wide set of models. The maximum attack success rate of our robustness scaling analysis resulted from either the category GeometricMasksV1 or GeometricMasksV2 for all evaluated models. For GeometricMasksV1, the Circle 140 variant consistently achieved the highest ASR across all models, whereas in GeometricMasksV2, the worst case was almost always the 6-7-2 C1 Opacity 128 variant, with 6-4-2 C1 Opacity 128 occasionally dominating. Notably, the same attack variant tended to yield the worst case of our attacks within entire model families, e.g., CLIP, DINOv2, SWIN, BEiT, BEiTv2, indicating that adversarial vulnerabilities are not randomly distributed but reflect systematic weaknesses tied to architectural or training similarities. From the perspective of an adversary, this means that even without precise knowledge of the deployed model, limited information about the model family can already guide the choice of attack: knowing the family suffices to select a

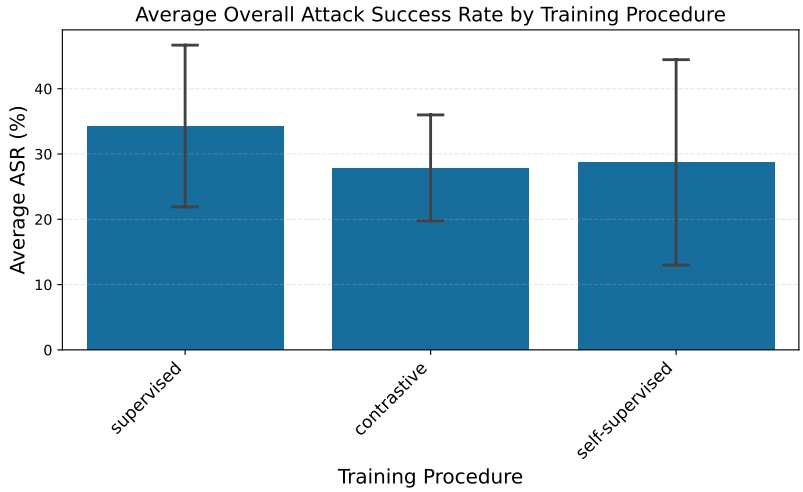

Figure 19: Average attack success rates by training procedure with standard deviation error bars

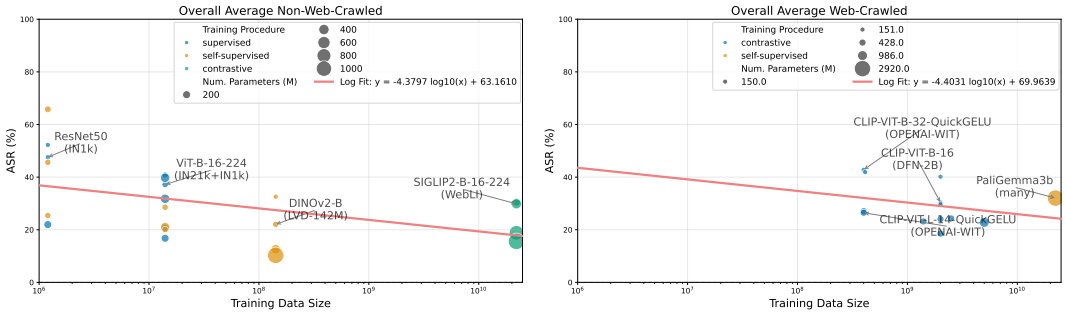

(a) Overall average non-web-crawled

(b) Overall average web-crawled

Figure 20: Robustness comparison between non-web-crawled and web-crawled datasets

variant that is likely to perform near-optimally across all its members. This family-level consistency substantially reduces the uncertainty an attacker would face in practice and highlights the need to consider family-specific robustness evaluations. Furthermore, these findings show that DINOv2 not only achieves strong robustness on average but also maintains resilience under worst-case adversarial scenarios, underscoring its relative reliability across both typical and extreme conditions.

G.5 Adversarial Fine-Tuning

The evaluation of fine-tuned ResNet50 models, alongside the vanilla ResNet50, reveals distinct patterns in how adversarial training with geometric masks influences model robustness and generalization capabilities. Figure 22 presents the Attack Success Rates (ASR) across various mask configurations, demonstrating the effectiveness of different training strategies. The accuracies of the fine-tuned models on the clean ImageNet validation dataset lie between 75% and 77%.

G.5.1 Generalization Across Opacity Levels

Fine-tuning with geometric masks demonstrates remarkable generalization across opacity levels for all models. The Model ResNet50-v1, trained on opacity 64, exhibits only slightly decreased performance when evaluated on opacity 128. In contrast, the vanilla ResNet50 displays an extreme vulnerability to opacity variations. This difference underscores the effectiveness of adversarial fine-tuning in creating opacity-invariant representations.

G.5.2 Structural Generalization

The fine-tuned models demonstrate robust generalization across geometric variations:

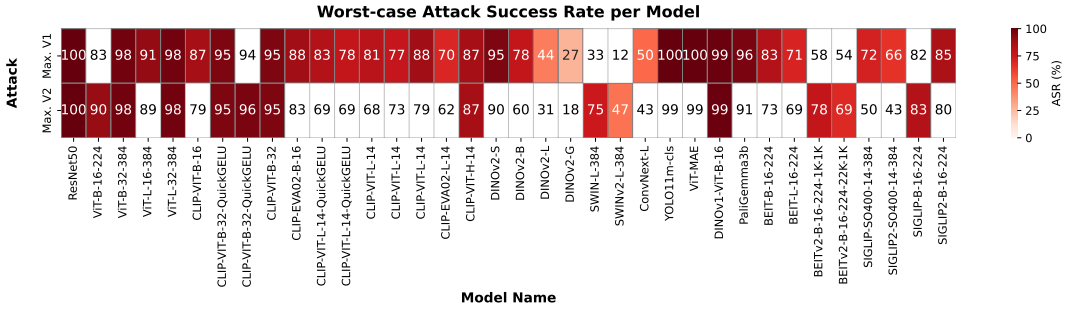

Figure 21: Worst-case attack success rate of the robustness analysis. "Max. V1" is the maximum ASR that occurred in the GeometricMasksV1 attack for a given model, where only the maximum is colored. "Max. V2" signifies GeometricMasksV2

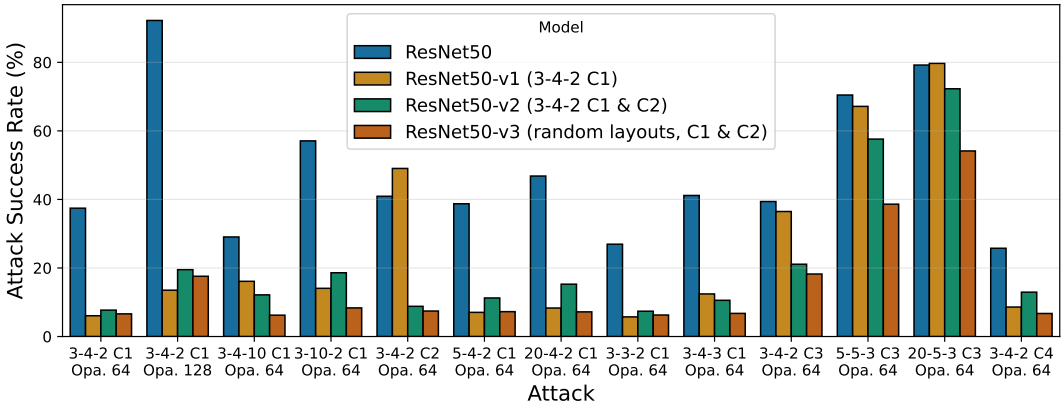

Figure 22: Attack success rate comparison between the vanilla ResNet50 and three fine-tuned variants on various GeometricMasksV2 attacks. The attacks are indicated by their masks (`a-b-c`), color scheme (C1, C2, C3, or C4), and the opacity of the masks.

Polygon sides Models maintain consistent performance across masks with varying polygon sides. The ASR remains low for both 5-sided (5-4-2 C1) and 20-sided (20-5-3 C1) polygon configurations, with all fine-tuned variants achieving ASRs below 16%, while the vanilla ResNet50 shows ASRs of 38.7% and 46.8%, respectively.

Polygons per row and column Varying the number of polygons per row and column has minimal impact on fine-tuned model performance. Masks 3-10-2 C1 (high column density) and 3-3-2 C1 (low density) yield similar ASRs across all fine-tuned models. In contrast, the high column density configuration resulted in the fourth highest ASR for the standard ResNet50.

Concentric polygons The models effectively generalize across different numbers of concentric layers, as evidenced by consistent performance on masks 3-4-10 C1 and 3-4-3 C1. Notably, on the 3-4-3 C1 mask, the attack success rate of the vanilla ResNet50 was 3.3 times higher than that of the worst-performing fine-tuned model, highlighting the robustness gains achieved through fine-tuning.

Rotation The 3-4-2 C4 configuration, rotated 45 degrees from the standard orientation, shows minimal performance degradation across fine-tuned models, indicating learned rotation-invariant features. However, it is essential to note that this was also the weakest attack against the vanilla ResNet50, with an ASR of only 25.8%, presumably because the mask does not cover the entire image.

G.5.3 Color Scheme Limitations

Color generalization represents the primary limitation of the fine-tuning approach. Models exhibit strong performance primarily on color schemes encountered during training:

Table 6: Accuracy (%) of models and humans at different opacity levels. These are the values shown in Figure 5.

Opacity level	0	64	96	128
ResNet50	99.90	89.32	52.05	26.17
ResNet50-v1 (3-4-2 C1)	99.85	99.13	**97.43**	87.16
ViT-B-16-224	99.72	98.24	90.04	59.49
CLIP-VIT-B-16	99.34	96.31	87.36	69.12
DINOv2-B	99.97	**99.26**	95.82	86.52
Avg. Humans	**100.00**	97.33	96.00	**93.33**

ResNet50-v1, trained exclusively on color scheme C1, shows elevated ASRs when evaluated on C2 and C3 color schemes. ResNet50-v2, trained on both C1 and C2 color schemes, demonstrates improved generalization with lower ASRs across both schemes. On the novel C3 color scheme (unseen during training), all fine-tuned models show degraded performance. However, the models v2 and v3 are less affected than v1.

ResNet50-v4, trained with random mask selection and dual color schemes, achieves the most consistent performance across all evaluations. On the configurations 5-5-3 C3 and 20-5-3 C3, which have all parameters different from those seen during training, ResNet50-v4 outperforms the other models by a significant margin of 18%, suggesting that diverse training conditions promote broader generalization.

These results indicate that while geometric and structural features can be effectively learned through adversarial fine-tuning, color-based robustness requires explicit exposure to diverse color schemes during training, highlighting the importance of comprehensive augmentation strategies.

G.6 Table with human and model performance

H Full Adversarial Robustness Evaluation Results

I Compute usage

The experiments were conducted on an internal cluster equipped with RTX 3090s and RTX 2080 TIs. In total, we have logged 322.5 GPU hours for the experiments and testing.

NeurIPS Paper Checklist

1. **Claims**

   Question: Do the main claims made in the abstract and introduction accurately reflect the paper's contributions and scope?

   Answer: [Yes]

   Justification:

   Guidelines:

   - The answer NA means that the abstract and introduction do not include the claims made in the paper.
   - The abstract and/or introduction should clearly state the claims made, including the contributions made in the paper and important assumptions and limitations. A No or NA answer to this question will not be perceived well by the reviewers.
   - The claims made should match theoretical and experimental results, and reflect how much the results can be expected to generalize to other settings.
   - It is fine to include aspirational goals as motivation as long as it is clear that these goals are not attained by the paper.

2. **Limitations**

Table 7: Baseline accuracies (%) for ImageNet1K-Val, ImageNet-200, and Images in COCO Objects

Model Name	Training Dataset	ImageNet1K-Val	ImageNet-200	Images in COCO Objects
ResNet50	IN1k	80.0	93.8	78.9
ViT-B-16-224	IN21k+IN1k	80.3	94.2	79.1
ViT-B-32-384	IN21k+IN1k	81.2	94.8	80.9
ViT-L-16-384	IN21k+IN1k	85.0	96.3	83.8
ViT-L-32-384	IN21k+IN1k	81.0	95.0	79.2
CLIP-VIT-B-16	DFN-2B	74.0	93.4	71.3
CLIP-VIT-B-32-QuickGELU	OPENAI-WIT	59.6	85.8	60.2
CLIP-VIT-B-32-QuickGELU	LAION-400M	59.4	84.7	55.1
CLIP-VIT-B-32	LAION-2B	63.7	87.6	62.4
CLIP-EVA02-B-16	LAION-2B(1.6B) + COYO-700M(400M)	72.6	93.3	71.2
CLIP-VIT-L-14-QuickGELU	MetaClip400M	72.3	92.3	70.4
CLIP-VIT-L-14-QuickGELU	OPENAI-WIT	70.8	92.7	69.8
CLIP-VIT-L-14	DataComp-1B	76.9	94.5	74.5
CLIP-VIT-L-14	MetaClip full CC	74.2	94.4	72.4
CLIP-VIT-L-14	DFN-2B	78.9	95.5	76.7
CLIP-EVA02-L-14	LAION-2B(1.6B) + COYO-700M(400M)	77.4	95.6	75.0
CLIP-VIT-H-14	DFN-5B	81.3	96.2	76.8
DINOv2-S	LVD-142M	80.9	94.5	79.6
DINOv2-B	LVD-142M	84.4	96.2	82.5
DINOv2-L	LVD-142M	86.2	97.2	84.5
DINOv2-G	LVD-142M	86.7	97.3	85.0
SWIN-L-384	IN1k	86.6	97.3	85.1
SWINv2-L-384	IN21k+IN1k	87.2	97.4	84.4
ConvNext-L	IN21k+IN1k	85.7	97.1	84.8
YOLO11m-cls	IN1k	77.3	92.8	76.8
ViT-MAE	IN1k	52.3	72.5	52.2
DINOv1-ViT-B-16	IN1k	75.9	91.9	75.0
PaliGemma3b	many	83.7	95.8	83.4
BEIT-B-16-224	IN21k+IN1k	84.5	96.4	83.5
BEIT-L-16-224	IN21k+IN1k	87.2	97.4	84.5
BEITv2-B-16-224-1K-1K	IN1k+IN1k	85.5	96.8	84.6
BEITv2-B-16-224-22K-1K	IN1k+(IN21k+IN1k)	86.2	97.1	84.7
SIGLIP-SO400-14-384	WebLI	80.8	96.3	79.9
SIGLIP2-SO400-14-384	WebLI	74.1	90.0	76.8
SIGLIP-B-16-224	WebLI	73.2	92.8	70.6
SIGLIP2-B-16-224	WebLI	69.2	87.9	70.6

Question: Does the paper discuss the limitations of the work performed by the authors?

Answer: [Yes]

Justification: As part of the conclusion.

Guidelines:

- The answer NA means that the paper has no limitation while the answer No means that the paper has limitations, but those are not discussed in the paper.
- The authors are encouraged to create a separate "Limitations" section in their paper.
- The paper should point out any strong assumptions and how robust the results are to violations of these assumptions (e.g., independence assumptions, noiseless settings, model well-specification, asymptotic approximations only holding locally). The authors should reflect on how these assumptions might be violated in practice and what the implications would be.
- The authors should reflect on the scope of the claims made, e.g., if the approach is only tested on a few datasets or with a few runs. In general, empirical results often depend on implicit assumptions, which should be articulated.
- The authors should reflect on the factors that influence the performance of the approach. For example, a facial recognition algorithm may perform poorly when image resolution is low or images are taken in low lighting. Or a speech-to-text system might not be used reliably to provide closed captions for online lectures because it fails to handle technical jargon.

Table 8: Attack success rates (%) for Random Attacks

Model Name	Training Dataset	Random Hue 0.5	Random Saturation 0.9	Random Contrast 0.9	Random Brightness 0.7	Avg. Random Perturbations
ResNet50	IN1k	14.6	2.3	2.8	10.0	7.4
ViT-B-16-224	IN21k+IN1k	18.8	4.2	6.6	16.7	11.6
ViT-B-32-384	IN21k+IN1k	16.8	3.7	5.5	15.4	10.3
ViT-L-16-384	IN21k+IN1k	12.8	2.8	4.6	11.8	8.0
ViT-L-32-384	IN21k+IN1k	19.4	4.7	7.4	16.5	12.0
CLIP-VIT-B-16	DFN-2B	16.0	3.6	4.3	13.8	9.4
CLIP-VIT-B-32-QuickGELU	OPENAI-WIT	27.5	7.6	9.4	20.8	16.3
CLIP-VIT-B-32-QuickGELU	LAION-400M	25.8	7.1	9.4	21.8	16.0
CLIP-VIT-B-32	LAION-2B	23.9	6.6	7.7	19.5	14.4
CLIP-EVA02-B-16	LAION-2B(1.6B) + COYO-700M(400M)	16.2	3.6	4.6	12.8	9.3
CLIP-VIT-L-14-QuickGELU	MetaClip400M	16.1	4.1	6.1	15.0	10.3
CLIP-VIT-L-14-QuickGELU	OPENAI-WIT	17.0	3.6	5.1	12.6	9.6
CLIP-VIT-L-14	DataComp-1B	13.4	2.7	3.3	10.5	7.5
CLIP-VIT-L-14	MetaClip full CC	14.5	3.5	5.3	13.8	9.3
CLIP-VIT-L-14	DFN-2B	10.8	2.2	3.1	9.7	6.5
CLIP-EVA02-L-14	LAION-2B(1.6B) + COYO-700M(400M)	11.5	2.3	3.5	8.7	6.5
CLIP-VIT-H-14	DFN-5B	8.7	1.9	2.7	8.7	5.5
DINOv2-S	LVD-142M	7.0	1.9	2.1	8.7	4.9
DINOv2-B	LVD-142M	4.3	1.3	1.3	6.1	3.2
DINOv2-L	LVD-142M	2.5	0.9	0.8	4.0	2.0
DINOv2-G	LVD-142M	2.1	0.8	0.8	3.8	1.9
SWIN-L-384	IN1k	7.2	1.2	1.4	4.7	3.6
SWINv2-L-384	IN21k+IN1k	6.7	0.9	1.1	3.9	3.2
ConvNext-L	IN21k+IN1k	7.7	2.2	2.4	6.2	4.6
YOLO11m-cls	IN1k	16.0	4.0	4.5	15.5	10.0
ViT-MAE	IN1k	33.6	8.3	13.7	30.0	21.4
DINOv1-ViT-B-16	IN1k	13.2	6.7	6.7	16.1	10.7
PaliGemma3b	many	11.5	2.5	3.9	12.2	7.5
BEIT-B-16-224	IN21k+IN1k	10.1	1.4	1.8	6.7	5.0
BEIT-L-16-224	IN21k+IN1k	6.5	1.0	1.0	4.6	3.3
BEITv2-B-16-224-1K-1K	IN1k+IN1k	7.7	1.2	1.5	5.8	4.1
BEITv2-B-16-224-22K-1K	IN1k+(IN21k+IN1k)	7.9	1.1	1.3	5.5	4.0
SIGLIP-SO400-14-384	WebLI	8.5	1.8	3.3	8.9	5.6
SIGLIP2-SO400-14-384	WebLI	6.3	1.4	2.0	4.5	3.6
SIGLIP-B-16-224	WebLI	15.3	3.8	6.5	16.1	10.4
SIGLIP2-B-16-224	WebLI	14.1	3.4	5.0	11.9	8.6

- The authors should discuss the computational efficiency of the proposed algorithms and how they scale with dataset size.
- If applicable, the authors should discuss possible limitations of their approach to address problems of privacy and fairness.
- While the authors might fear that complete honesty about limitations might be used by reviewers as grounds for rejection, a worse outcome might be that reviewers discover limitations that aren't acknowledged in the paper. The authors should use their best judgment and recognize that individual actions in favor of transparency play an important role in developing norms that preserve the integrity of the community. Reviewers will be specifically instructed to not penalize honesty concerning limitations.

3. **Theory assumptions and proofs**

   Question: For each theoretical result, does the paper provide the full set of assumptions and a complete (and correct) proof?

   Answer: [NA]

   Justification:

   Guidelines:

   - The answer NA means that the paper does not include theoretical results.
   - All the theorems, formulas, and proofs in the paper should be numbered and cross-referenced.
   - All assumptions should be clearly stated or referenced in the statement of any theorems.
   - The proofs can either appear in the main paper or the supplemental material, but if they appear in the supplemental material, the authors are encouraged to provide a short proof sketch to provide intuition.
   - Inversely, any informal proof provided in the core of the paper should be complemented by formal proofs provided in appendix or supplemental material.

Table 9: Attack success rates (%) for GeometricMasksV1

Model Name	Training Dataset	GeometricMasksV1 Circle 50	GeometricMasksV1 Circle 80	GeometricMasksV1 Circle 110	GeometricMasksV1 Circle 140	Avg. GeometricMasksV1
ResNet50	IN1k	40.5	83.7	97.7	99.6	80.4
ViT-B-16-224	IN21k+IN1k	15.1	29.4	55.0	83.4	45.7
ViT-B-32-384	IN21k+IN1k	24.1	55.3	85.0	97.7	65.5
ViT-L-16-384	IN21k+IN1k	16.8	39.0	69.0	91.1	54.0
ViT-L-32-384	IN21k+IN1k	23.9	51.8	83.3	97.5	64.1
CLIP-VIT-B-16	DFN-2B	18.3	39.7	65.5	86.6	52.5
CLIP-VIT-B-32-QuickGELU	OPENAI-WIT	36.0	62.1	83.2	95.3	69.2
CLIP-VIT-B-32-QuickGELU	LAION-400M	27.3	53.8	78.8	94.1	63.5
CLIP-VIT-B-32	LAION-2B	27.9	55.2	80.9	95.1	64.8
CLIP-EVA02-B-16	LAION-2B(1.6B) + COYO-700M(400M)	19.8	40.5	65.5	88.4	53.6
CLIP-VIT-L-14-QuickGELU	MetaClip400M	23.2	43.2	63.8	83.0	53.3
CLIP-VIT-L-14-QuickGELU	OPENAI-WIT	25.6	43.3	60.5	78.2	51.9
CLIP-VIT-L-14	DataComp-1B	17.4	35.6	58.0	80.9	48.0
CLIP-VIT-L-14	MetaClip full CC	18.8	35.3	55.6	77.3	46.7
CLIP-VIT-L-14	DFN-2B	15.0	35.5	63.2	87.7	50.4
CLIP-EVA02-L-14	LAION-2B(1.6B) + COYO-700M(400M)	11.6	24.9	44.9	69.8	37.8
CLIP-VIT-H-14	DFN-5B	11.8	30.9	59.6	86.8	47.3
DINOv2-S	LVD-142M	20.2	47.9	77.7	95.0	60.2
DINOv2-B	LVD-142M	11.4	26.7	51.7	77.8	41.9
DINOv2-L	LVD-142M	5.7	11.6	23.8	43.6	21.2
DINOv2-G	LVD-142M	4.7	8.0	14.4	26.6	13.4
SWIN-L-384	IN1k	8.2	11.7	19.5	32.5	18.0
SWINv2-L-384	IN21k+IN1k	6.8	8.8	10.2	12.2	9.5
ConvNext-L	IN21k+IN1k	13.7	25.9	37.8	49.6	31.8
YOLO11m-cls	IN1k	50.4	90.8	98.9	99.7	85.0
ViT-MAE	IN1k	68.5	94.4	99.0	99.6	90.4
DINOv1-ViT-B-16	IN1k	30.1	66.4	92.2	98.9	71.9
PaliGemma3b	many	26.1	59.5	84.7	96.5	66.7
BEIT-B-16-224	IN21k+IN1k	12.7	29.9	56.9	83.2	45.7
BEIT-L-16-224	IN21k+IN1k	8.9	20.5	41.8	71.0	35.5
BEITv2-B-16-224-1K-1K	IN1k+IN1k	11.0	19.7	34.5	58.4	30.9
BEITv2-B-16-224-22K-1K	IN1k+(IN21k+IN1k)	7.0	11.5	24.5	54.4	24.4
SIGLIP-SO400-14-384	WebLI	13.0	28.1	48.7	71.7	40.4
SIGLIP2-SO400-14-384	WebLI	11.8	24.0	42.0	65.9	35.9
SIGLIP-B-16-224	WebLI	12.8	28.0	54.7	81.8	44.3
SIGLIP2-B-16-224	WebLI	15.8	34.7	61.8	85.4	49.4

Table 10: Attack success rates (%) for GeometricMasksV2

Model Name	Training Dataset	GeometricMasksV2 3-4-2 C1 Opacity 64	GeometricMasksV2 3-4-2 C1 Opacity 96	GeometricMasksV2 3-4-2 C1 Opacity 128	GeometricMasksV2 3-4-5 C1 Opacity 128	GeometricMasksV2 3-7-2 C1 Opacity 128	GeometricMasksV2 6-4-2 C1 Opacity 128	GeometricMasksV2 6-7-2 C1 Opacity 128	Avg. GeometricMasksV2
ResNet50	IN1k	33.7	62.1	92.2	87.7	99.1	99.0	99.6	81.9
ViT-B-16-224	IN21k+IN1k	23.8	40.3	58.5	51.5	80.6	90.4	88.1	61.9
ViT-B-32-384	IN21k+IN1k	16.3	33.8	58.6	53.2	94.5	88.1	98.4	63.3
ViT-L-16-384	IN21k+IN1k	14.2	21.9	33.0	31.2	52.8	66.6	89.2	44.1
ViT-L-32-384	IN21k+IN1k	18.5	34.5	57.7	52.1	89.0	85.4	98.5	62.2
CLIP-VIT-B-16	DFN-2B	18.3	27.8	38.8	40.5	64.8	66.4	78.9	47.9
CLIP-VIT-B-32-QuickGELU	OPENAI-WIT	41.7	56.1	68.3	70.5	90.7	89.5	95.5	73.2
CLIP-VIT-B-32-QuickGELU	LAION-400M	39.0	58.4	80.4	76.9	93.3	96.2	92.8	76.7
CLIP-VIT-B-32	LAION-2B	34.2	52.4	69.0	68.4	91.8	89.9	94.8	71.5
CLIP-EVA02-B-16	LAION-2B(1.6B) + COYO-700M(400M)	20.5	29.7	40.0	44.4	69.0	71.0	83.5	51.2
CLIP-VIT-L-14-QuickGELU	MetaClip400M	17.2	22.7	28.8	30.8	43.1	48.8	69.0	37.2
CLIP-VIT-L-14-QuickGELU	OPENAI-WIT	18.9	25.5	32.4	36.4	43.7	46.3	68.9	38.9
CLIP-VIT-L-14	DataComp-1B	15.8	22.4	28.7	29.3	42.3	44.6	67.7	35.8
CLIP-VIT-L-14	MetaClip full CC	14.1	19.6	25.8	26.8	37.0	51.3	72.7	35.3
CLIP-VIT-L-14	DFN-2B	11.2	18.4	27.3	28.4	47.5	53.2	79.0	37.9
CLIP-EVA02-L-14	LAION-2B(1.6B) + COYO-700M(400M)	10.1	15.2	21.8	22.3	34.2	42.4	62.2	29.7
CLIP-VIT-H-14	DFN-5B	8.9	15.3	24.2	24.1	52.6	64.8	87.4	39.6
DINOv2-S	LVD-142M	13.2	17.4	26.3	26.3	50.9	53.5	90.1	39.7
DINOv2-B	LVD-142M	7.5	9.3	12.6	12.7	22.9	28.2	60.2	21.9
DINOv2-L	LVD-142M	4.4	5.2	6.4	7.0	10.6	11.5	31.1	10.9
DINOv2-G	LVD-142M	3.8	4.6	5.8	6.1	8.6	9.8	18.3	8.1
SWIN-L-384	IN1k	9.6	12.3	15.8	17.6	67.6	53.6	75.3	36.0
SWINv2-L-384	IN21k+IN1k	5.8	6.7	7.9	8.2	25.8	17.6	47.2	17.0
ConvNext-L	IN21k+IN1k	8.2	11.4	15.9	20.6	18.7	30.2	43.2	21.2
YOLO11m-cls	IN1k	31.7	58.8	82.0	91.6	97.7	91.3	98.7	78.8
ViT-MAE	IN1k	58.8	81.2	92.8	94.9	98.7	98.0	99.2	89.1
DINOv1-ViT-B-16	IN1k	29.5	46.7	63.0	63.2	90.6	92.4	98.9	69.2
PaliGemma3b	many	17.1	26.5	38.5	46.2	68.3	69.8	91.4	51.1
BEIT-B-16-224	IN21k+IN1k	13.2	21.3	31.1	34.5	67.0	71.0	73.2	44.5
BEIT-L-16-224	IN21k+IN1k	8.6	12.4	17.2	17.4	42.4	63.1	69.0	32.9
BEITv2-B-16-224-1K-1K	IN1k+IN1k	8.8	12.9	17.9	19.6	32.4	77.9	68.7	34.0
BEITv2-B-16-224-22K-1K	IN1k+(IN21k+IN1k)	5.7	9.4	20.7	18.5	29.8	49.9	69.0	29.0
SIGLIP-SO400-14-384	WebLI	7.9	11.8	16.5	18.9	27.9	28.8	50.4	23.2
SIGLIP2-SO400-14-384	WebLI	9.3	12.1	16.0	16.2	24.6	22.0	43.1	20.5
SIGLIP-B-16-224	WebLI	22.2	34.1	47.7	48.1	79.1	73.7	83.1	55.5
SIGLIP2-B-16-224	WebLI	23.1	35.1	47.7	46.6	76.6	74.5	79.9	54.8

- Theorems and Lemmas that the proof relies upon should be properly referenced.

4. **Experimental result reproducibility**

   Question: Does the paper fully disclose all the information needed to reproduce the main experimental results of the paper to the extent that it affects the main claims and/or conclusions of the paper (regardless of whether the code and data are provided or not)?

   Answer: [Yes]

   Justification: We run the models using the standard setups and will provide the codebase.

   Guidelines:

   - The answer NA means that the paper does not include experiments.
   - If the paper includes experiments, a No answer to this question will not be perceived well by the reviewers: Making the paper reproducible is important, regardless of whether the code and data are provided or not.
   - If the contribution is a dataset and/or model, the authors should describe the steps taken to make their results reproducible or verifiable.

Table 11: Attack success rates (%) for COCO Objects

Model Name	Training Dataset	COCO Objects Black Background	COCO Objects Thresholded Perlin Noise Background	COCO Objects Perlin Noise Background	Avg. COCO Objects
ResNet50	IN1k	18.3	18.6	22.3	19.7
ViT-B-16-224	IN21k+IN1k	24.3	25.5	36.0	28.6
ViT-B-32-384	IN21k+IN1k	21.0	23.8	32.7	25.8
ViT-L-16-384	IN21k+IN1k	15.0	17.6	29.2	20.6
ViT-L-32-384	IN21k+IN1k	20.8	24.4	35.7	27.0
CLIP-VIT-B-16	DFN-2B	20.5	22.8	27.6	23.7
CLIP-VIT-B-32-QuickGELU	OPENAI-WIT	28.5	37.8	41.2	35.8
CLIP-VIT-B-32-QuickGELU	LAION-400M	30.3	36.7	41.6	36.2
CLIP-VIT-B-32	LAION-2B	29.4	33.8	36.8	33.3
CLIP-EVA02-B-16	LAION-2B(1.6B) + COYO-700M(400M)	18.6	19.9	23.4	20.6
CLIP-VIT-L-14-QuickGELU	MetaClip400M	20.5	22.0	27.5	23.4
CLIP-VIT-L-14-QuickGELU	OPENAI-WIT	16.5	22.6	28.8	22.6
CLIP-VIT-L-14	DataComp-1B	16.0	17.9	20.2	18.0
CLIP-VIT-L-14	MetaClip full CC	19.0	21.0	24.0	21.3
CLIP-VIT-L-14	DFN-2B	16.4	17.9	21.4	18.6
CLIP-EVA02-L-14	LAION-2B(1.6B) + COYO-700M(400M)	13.6	15.8	17.2	15.5
CLIP-VIT-H-14	DFN-5B	14.4	16.2	20.9	17.2
DINOv2-S	LVD-142M	17.4	21.3	26.2	21.6
DINOv2-B	LVD-142M	12.9	17.5	17.6	16.0
DINOv2-L	LVD-142M	9.4	12.0	10.7	10.7
DINOv2-G	LVD-142M	8.2	13.2	10.8	10.7
SWIN-L-384	IN1k	8.6	26.8	41.5	25.6
SWINv2-L-384	IN21k+IN1k	8.1	30.1	36.4	24.9
ConvNext-L	IN21k+IN1k	12.1	12.7	16.9	13.9
YOLO11m-cls	IN1k	21.7	30.0	38.9	30.2
ViT-MAE	IN1k	46.5	54.6	80.6	60.5
DINOv1-ViT-B-16	IN1k	19.5	22.8	32.2	24.8
PaliGemma3b	many	16.2	19.3	23.0	19.5
BEIT-B-16-224	IN21k+IN1k	16.7	17.4	27.8	20.7
BEIT-L-16-224	IN21k+IN1k	11.4	13.2	21.2	15.3
BEITv2-B-16-224-1K-1K	IN1k+IN1k	9.8	15.1	61.1	28.7
BEITv2-B-16-224-22K-1K	IN1k+(IN21k+IN1k)	10.8	11.8	23.9	15.5
SIGLIP-SO400-14-384	WebLI	12.0	14.7	18.2	15.0
SIGLIP2-SO400-14-384	WebLI	9.8	13.4	14.7	12.6
SIGLIP-B-16-224	WebLI	23.9	26.0	32.0	27.3
SIGLIP2-B-16-224	WebLI	21.1	25.1	28.4	24.8

- Depending on the contribution, reproducibility can be accomplished in various ways. For example, if the contribution is a novel architecture, describing the architecture fully might suffice, or if the contribution is a specific model and empirical evaluation, it may be necessary to either make it possible for others to replicate the model with the same dataset, or provide access to the model. In general. releasing code and data is often one good way to accomplish this, but reproducibility can also be provided via detailed instructions for how to replicate the results, access to a hosted model (e.g., in the case of a large language model), releasing of a model checkpoint, or other means that are appropriate to the research performed.
- While NeurIPS does not require releasing code, the conference does require all submissions to provide some reasonable avenue for reproducibility, which may depend on the nature of the contribution. For example
  (a) If the contribution is primarily a new algorithm, the paper should make it clear how to reproduce that algorithm.
  (b) If the contribution is primarily a new model architecture, the paper should describe the architecture clearly and fully.
  (c) If the contribution is a new model (e.g., a large language model), then there should either be a way to access this model for reproducing the results or a way to reproduce the model (e.g., with an open-source dataset or instructions for how to construct the dataset).
  (d) We recognize that reproducibility may be tricky in some cases, in which case authors are welcome to describe the particular way they provide for reproducibility. In the case of closed-source models, it may be that access to the model is limited in

Table 12: Attack success rates (%)for ImageNet-C approximated using ImageNet-1K

Model Name	Training Dataset	ImageNet-C Distortion Severity 1	ImageNet-C Distortion Severity 2	ImageNet-C Distortion Severity 3	ImageNet-C Distortion Severity 4	ImageNet-C Distortion Severity 5	Avg. ImageNet-C
ResNet50	IN1k	16.4	26.9	36.9	50.9	65.4	39.3
ViT-B-16-224	IN21k+IN1k	7.1	14.4	20.8	33.0	50.1	25.1
ViT-B-32-384	IN21k+IN1k	8.7	16.1	22.2	35.3	52.1	26.9
ViT-L-16-384	IN21k+IN1k	7.7	13.1	17.7	26.8	41.3	21.3
ViT-L-32-384	IN21k+IN1k	7.7	14.3	19.5	30.1	46.1	23.5
CLIP-VIT-B-16	DFN-2B	12.1	22.5	30.8	43.3	57.7	33.3
CLIP-VIT-B-32-QuickGELU	OPENAI-WIT	12.8	23.1	32.8	47.0	62.4	35.6
CLIP-VIT-B-32-QuickGELU	LAION-400M	15.5	26.6	35.9	49.7	64.2	38.4
CLIP-VIT-B-32	LAION-2B	15.0	25.8	35.0	48.4	63.1	37.5
CLIP-EVA02-B-16	LAION-2B(1.6B) + COYO-700M(400M)	8.2	16.1	23.6	34.7	49.7	26.5
CLIP-VIT-L-14-QuickGELU	MetaClip400M	10.4	18.7	25.8	37.9	51.6	28.9
CLIP-VIT-L-14-QuickGELU	OPENAI-WIT	8.7	15.6	21.9	32.1	45.5	24.8
CLIP-VIT-L-14	DataComp-1B	7.2	13.2	18.8	28.3	40.8	21.7
CLIP-VIT-L-14	MetaClip full CC	8.5	16.1	22.0	32.4	45.5	24.9
CLIP-VIT-L-14	DFN-2B	6.7	13.5	19.3	28.7	41.6	22.0
CLIP-EVA02-L-14	LAION-2B(1.6B) + COYO-700M(400M)	5.4	9.4	13.2	19.4	29.6	15.4
CLIP-VIT-H-14	DFN-5B	6.4	12.2	17.5	26.0	39.3	20.3
DINOv2-S	LVD-142M	9.2	17.2	24.9	37.0	53.3	28.3
DINOv2-B	LVD-142M	6.0	11.1	16.2	24.9	38.4	19.3
DINOv2-L	LVD-142M	3.6	6.7	9.2	14.2	23.4	11.4
DINOv2-G	LVD-142M	3.3	6.1	7.9	11.7	19.0	9.6
SWIN-L-384	IN1k	7.6	11.1	15.5	21.3	31.5	17.4
SWINv2-L-384	IN21k+IN1k	7.1	11.0	14.6	19.7	29.4	16.4
ConvNext-L	IN21k+IN1k	8.2	13.4	17.5	24.7	35.5	19.9
YOLO11m-cls	IN1k	25.4	39.6	51.7	65.9	77.8	52.1
ViT-MAE	IN1k	30.3	45.5	56.9	69.9	81.7	56.9
DINOv1-ViT-B-16	IN1k	11.7	21.9	32.7	47.4	63.8	35.5
PaliGemma3b	many	11.0	20.5	29.6	42.5	57.5	32.2
BEIT-B-16-224	IN21k+IN1k	6.5	11.3	15.9	23.9	37.0	18.9
BEIT-L-16-224	IN21k+IN1k	4.6	7.9	10.5	15.6	25.4	12.8
BEITv2-B-16-224-1K-1K	IN1k+IN1k	7.7	12.1	17.4	24.6	36.2	19.6
BEITv2-B-16-224-22K-1K	IN1k+(IN21k+IN1k)	6.6	11.2	14.5	20.7	31.1	16.8
SIGLIP-SO400-14-384	WebLI	7.7	14.4	20.9	31.3	44.7	23.8
SIGLIP2-SO400-14-384	WebLI	4.3	8.7	13.8	22.3	34.6	16.7
SIGLIP-B-16-224	WebLI	14.0	25.8	36.0	48.8	63.1	37.5
SIGLIP2-B-16-224	WebLI	11.0	21.7	30.5	42.7	56.7	32.5

some way (e.g., to registered users), but it should be possible for other researchers to have some path to reproducing or verifying the results.

5. **Open access to data and code**

   Question: Does the paper provide open access to the data and code, with sufficient instructions to faithfully reproduce the main experimental results, as described in supplemental material?

   Answer: [Yes]

   Justification: The code is provided in a zip file

   Guidelines:

   - The answer NA means that paper does not include experiments requiring code.
   - Please see the NeurIPS code and data submission guidelines (`https://nips.cc/public/guides/CodeSubmissionPolicy`) for more details.
   - While we encourage the release of code and data, we understand that this might not be possible, so "No" is an acceptable answer. Papers cannot be rejected simply for not including code, unless this is central to the contribution (e.g., for a new open-source benchmark).
   - The instructions should contain the exact command and environment needed to run to reproduce the results. See the NeurIPS code and data submission guidelines (`https://nips.cc/public/guides/CodeSubmissionPolicy`) for more details.
   - The authors should provide instructions on data access and preparation, including how to access the raw data, preprocessed data, intermediate data, and generated data, etc.
   - The authors should provide scripts to reproduce all experimental results for the new proposed method and baselines. If only a subset of experiments are reproducible, they should state which ones are omitted from the script and why.
   - At submission time, to preserve anonymity, the authors should release anonymized versions (if applicable).
   - Providing as much information as possible in supplemental material (appended to the paper) is recommended, but including URLs to data and code is permitted.

Table 13: Attack success rates (%) for ImageNet-R approximated using ImageNet-200

Model Name	Training Dataset	ImageNet-R
ResNet50	IN1k	56.5
ViT-B-16-224	IN21k+IN1k	50.2
ViT-B-32-384	IN21k+IN1k	52.7
ViT-L-16-384	IN21k+IN1k	42.6
ViT-L-32-384	IN21k+IN1k	49.3
CLIP-VIT-B-16	DFN-2B	15.3
CLIP-VIT-B-32-QuickGELU	OPENAI-WIT	26.7
CLIP-VIT-B-32-QuickGELU	LAION-400M	20.4
CLIP-VIT-B-32	LAION-2B	19.5
CLIP-EVA02-B-16	LAION-2B(1.6B) + COYO-700M(400M)	17.0
CLIP-VIT-L-14-QuickGELU	MetaClip400M	9.5
CLIP-VIT-L-14-QuickGELU	OPENAI-WIT	11.0
CLIP-VIT-L-14	DataComp-1B	7.8
CLIP-VIT-L-14	MetaClip full CC	8.3
CLIP-VIT-L-14	DFN-2B	9.0
CLIP-EVA02-L-14	LAION-2B(1.6B) + COYO-700M(400M)	6.3
CLIP-VIT-H-14	DFN-5B	6.9
DINOv2-S	LVD-142M	40.7
DINOv2-B	LVD-142M	30.0
DINOv2-L	LVD-142M	19.4
DINOv2-G	LVD-142M	17.9
SWIN-L-384	IN1k	31.2
SWINv2-L-384	IN21k+IN1k	29.7
ConvNext-L	IN21k+IN1k	32.6
YOLO11m-cls	IN1k	57.4
ViT-MAE	IN1k	76.3
DINOv1-ViT-B-16	IN1k	61.6
PaliGemma3b	many	15.1
BEIT-B-16-224	IN21k+IN1k	36.6
BEIT-L-16-224	IN21k+IN1k	26.3
BEITv2-B-16-224-1K-1K	IN1k+IN1k	35.2
BEITv2-B-16-224-22K-1K	IN1k+(IN21k+IN1k)	30.8
SIGLIP-SO400-14-384	WebLI	5.1
SIGLIP2-SO400-14-384	WebLI	4.0
SIGLIP-B-16-224	WebLI	8.0
SIGLIP2-B-16-224	WebLI	8.8

6. **Experimental setting/details**

   Question: Does the paper specify all the training and test details (e.g., data splits, hyper-parameters, how they are chosen, type of optimizer, etc.) necessary to understand the results?

   Answer: [Yes]

   Justification:

   Guidelines:

   - The answer NA means that the paper does not include experiments.
   - The experimental setting should be presented in the core of the paper to a level of detail that is necessary to appreciate the results and make sense of them.
   - The full details can be provided either with the code, in appendix, or as supplemental material.

7. **Experiment statistical significance**

   Question: Does the paper report error bars suitably and correctly defined or other appropriate information about the statistical significance of the experiments?

   Answer: [No]

   Justification:

   Guidelines:

   - The answer NA means that the paper does not include experiments.
   - The authors should answer "Yes" if the results are accompanied by error bars, confidence intervals, or statistical significance tests, at least for the experiments that support the main claims of the paper.
   - The factors of variability that the error bars are capturing should be clearly stated (for example, train/test split, initialization, random drawing of some parameter, or overall run with given experimental conditions).
   - The method for calculating the error bars should be explained (closed form formula, call to a library function, bootstrap, etc.)
   - The assumptions made should be given (e.g., Normally distributed errors).
   - It should be clear whether the error bar is the standard deviation or the standard error of the mean.
   - It is OK to report 1-sigma error bars, but one should state it. The authors should preferably report a 2-sigma error bar than state that they have a 96% CI, if the hypothesis of Normality of errors is not verified.
   - For asymmetric distributions, the authors should be careful not to show in tables or figures symmetric error bars that would yield results that are out of range (e.g. negative error rates).
   - If error bars are reported in tables or plots, The authors should explain in the text how they are calculated and reference the corresponding figures or tables in the text.

8. **Experiments compute resources**

   Question: For each experiment, does the paper provide sufficient information on the computer resources (type of compute workers, memory, time of execution) needed to reproduce the experiments?

   Answer: [Yes]

   Justification: See overall numbers in Appendix I.

   Guidelines:

   - The answer NA means that the paper does not include experiments.
   - The paper should indicate the type of compute workers CPU or GPU, internal cluster, or cloud provider, including relevant memory and storage.
   - The paper should provide the amount of compute required for each of the individual experimental runs as well as estimate the total compute.
   - The paper should disclose whether the full research project required more compute than the experiments reported in the paper (e.g., preliminary or failed experiments that didn't make it into the paper).

9. **Code of ethics**

   Question: Does the research conducted in the paper conform, in every respect, with the NeurIPS Code of Ethics `https://neurips.cc/public/EthicsGuidelines`?

   Answer: [Yes]

   Justification:

   Guidelines:

   - The answer NA means that the authors have not reviewed the NeurIPS Code of Ethics.
   - If the authors answer No, they should explain the special circumstances that require a deviation from the Code of Ethics.

- The authors should make sure to preserve anonymity (e.g., if there is a special consideration due to laws or regulations in their jurisdiction).

10. **Broader impacts**

    Question: Does the paper discuss both potential positive societal impacts and negative societal impacts of the work performed?

    Answer: [NA]

    Justification: There are no direct impacts from this work.

    Guidelines:

    - The answer NA means that there is no societal impact of the work performed.
    - If the authors answer NA or No, they should explain why their work has no societal impact or why the paper does not address societal impact.
    - Examples of negative societal impacts include potential malicious or unintended uses (e.g., disinformation, generating fake profiles, surveillance), fairness considerations (e.g., deployment of technologies that could make decisions that unfairly impact specific groups), privacy considerations, and security considerations.
    - The conference expects that many papers will be foundational research and not tied to particular applications, let alone deployments. However, if there is a direct path to any negative applications, the authors should point it out. For example, it is legitimate to point out that an improvement in the quality of generative models could be used to generate deepfakes for disinformation. On the other hand, it is not needed to point out that a generic algorithm for optimizing neural networks could enable people to train models that generate Deepfakes faster.
    - The authors should consider possible harms that could arise when the technology is being used as intended and functioning correctly, harms that could arise when the technology is being used as intended but gives incorrect results, and harms following from (intentional or unintentional) misuse of the technology.
    - If there are negative societal impacts, the authors could also discuss possible mitigation strategies (e.g., gated release of models, providing defenses in addition to attacks, mechanisms for monitoring misuse, mechanisms to monitor how a system learns from feedback over time, improving the efficiency and accessibility of ML).

11. **Safeguards**

    Question: Does the paper describe safeguards that have been put in place for responsible release of data or models that have a high risk for misuse (e.g., pretrained language models, image generators, or scraped datasets)?

    Answer: [NA]

    Justification:

    Guidelines:

    - The answer NA means that the paper poses no such risks.
    - Released models that have a high risk for misuse or dual-use should be released with necessary safeguards to allow for controlled use of the model, for example by requiring that users adhere to usage guidelines or restrictions to access the model or implementing safety filters.
    - Datasets that have been scraped from the Internet could pose safety risks. The authors should describe how they avoided releasing unsafe images.
    - We recognize that providing effective safeguards is challenging, and many papers do not require this, but we encourage authors to take this into account and make a best faith effort.

12. **Licenses for existing assets**

    Question: Are the creators or original owners of assets (e.g., code, data, models), used in the paper, properly credited and are the license and terms of use explicitly mentioned and properly respected?

    Answer: [Yes]

Justification:

Guidelines:

- The answer NA means that the paper does not use existing assets.
- The authors should cite the original paper that produced the code package or dataset.
- The authors should state which version of the asset is used and, if possible, include a URL.
- The name of the license (e.g., CC-BY 4.0) should be included for each asset.
- For scraped data from a particular source (e.g., website), the copyright and terms of service of that source should be provided.
- If assets are released, the license, copyright information, and terms of use in the package should be provided. For popular datasets, `paperswithcode.com/datasets` has curated licenses for some datasets. Their licensing guide can help determine the license of a dataset.
- For existing datasets that are re-packaged, both the original license and the license of the derived asset (if it has changed) should be provided.
- If this information is not available online, the authors are encouraged to reach out to the asset's creators.

13. **New assets**

    Question: Are new assets introduced in the paper well documented and is the documentation provided alongside the assets?

    Answer: [NA]

    Justification:

    Guidelines:

    - The answer NA means that the paper does not release new assets.
    - Researchers should communicate the details of the dataset/code/model as part of their submissions via structured templates. This includes details about training, license, limitations, etc.
    - The paper should discuss whether and how consent is obtained from people whose asset is used.
    - At submission time, remember to anonymize your assets (if applicable). You can either create an anonymized URL or include an anonymized zip file.

14. **Crowdsourcing and research with human subjects**

    Question: For crowdsourcing experiments and research with human subjects, does the paper include the full text of instructions given to participants and screenshots, if applicable, as well as details about compensation (if any)?

    Answer: [Yes]

    Justification: See Figure 15. Human volunteers are used for a small-scale experiment to annotate images and validate that the masks by Jabary et al. [30] are semantic preserving.

    Guidelines:

    - The answer NA means that the paper does not involve crowdsourcing nor research with human subjects.
    - Including this information in the supplemental material is fine, but if the main contribution of the paper involves human subjects, then as much detail as possible should be included in the main paper.
    - According to the NeurIPS Code of Ethics, workers involved in data collection, curation, or other labor should be paid at least the minimum wage in the country of the data collector.

15. **Institutional review board (IRB) approvals or equivalent for research with human subjects**

    Question: Does the paper describe potential risks incurred by study participants, whether such risks are disclosed to the subjects, and whether Institutional Review Board (IRB) approvals (or an equivalent approval/review based on the requirements of your country or institution) are obtained?

Answer: [NA]

Justification:

Guidelines:

- The answer NA means that the paper does not involve crowdsourcing nor research with human subjects.
- Depending on the country in which research is conducted, IRB approval (or equivalent) may be required for any human subjects research. If you obtained IRB approval, you should clearly state this in the paper.
- We recognize that the procedures for this may vary significantly between institutions and locations, and we expect authors to adhere to the NeurIPS Code of Ethics and the guidelines for their institution.
- For initial submissions, do not include any information that would break anonymity (if applicable), such as the institution conducting the review.

16. **Declaration of LLM usage**

Question: Does the paper describe the usage of LLMs if it is an important, original, or non-standard component of the core methods in this research? Note that if the LLM is used only for writing, editing, or formatting purposes and does not impact the core methodology, scientific rigorousness, or originality of the research, declaration is not required.

Answer: [NA]

Justification:

Guidelines:

- The answer NA means that the core method development in this research does not involve LLMs as any important, original, or non-standard components.
- Please refer to our LLM policy (`https://neurips.cc/Conferences/2025/LLM`) for what should or should not be described.

Table 14: Average attack success rates (%) of models on the different attacks classes.

Model Name	Training Dataset	Training Procedure	Training Data Size (M)	Random Perturbations	GeometricMasks V1	GeometricMasks V2	COCO Objects	ImageNet-C	Overall
ResNet50	IN1k	supervised	1.2	7.4	80.4	81.9	19.7	39.3	45.8
ViT-B-16-224	IN21k+IN1k	supervised	14.0	11.6	45.7	61.9	28.6	25.1	34.6
ViT-B-32-384	IN21k+IN1k	supervised	14.0	10.3	65.5	63.3	25.8	26.9	38.4
ViT-L-16-384	IN21k+IN1k	supervised	14.0	8.0	54.0	44.1	20.6	21.3	29.6
ViT-L-32-384	IN21k+IN1k	supervised	14.0	12.0	64.1	62.2	27.0	23.5	37.8
CLIP-VIT-B-16	DFN-2B	contrastive	2000.0	9.4	52.5	47.9	23.7	33.3	33.4
CLIP-VIT-B-32-QuickGELU	OPENAI-WIT	contrastive	400.0	16.3	69.2	73.2	35.8	35.6	46.0
CLIP-VIT-B-32-QuickGELU	LAION-400M	contrastive	413.0	16.0	63.5	76.7	36.2	38.4	46.2
CLIP-VIT-B-32	LAION-2B	contrastive	2000.0	14.4	64.8	71.5	33.3	37.5	44.3
CLIP-EVA02-B-16	LAION-2B(1.6B) + COYO-700M(400M)	contrastive	2000.0	9.3	53.6	51.2	20.6	26.5	32.2
CLIP-VIT-L-14-QuickGELU	MetaClip400M	contrastive	400.0	10.3	53.3	37.2	23.4	28.9	30.6
CLIP-VIT-L-14-QuickGELU	OPENAI-WIT	contrastive	400.0	9.6	51.9	38.9	22.6	24.8	29.5
CLIP-VIT-L-14	DataComp-1B	contrastive	1400.0	7.5	48.0	35.8	18.0	21.7	26.2
CLIP-VIT-L-14	MetaClip full CC	contrastive	2500.0	9.3	46.7	35.3	21.3	24.9	27.5
CLIP-VIT-L-14	DFN-2B	contrastive	2000.0	6.5	50.4	37.9	18.6	22.0	27.0
CLIP-EVA02-L-14	LAION-2B(1.6B) + COYO-700M(400M)	contrastive	2000.0	6.5	37.8	29.7	15.5	15.4	21.0
CLIP-VIT-H-14	DFN-5B	contrastive	5000.0	5.5	47.3	39.6	17.2	20.3	26.0
DINOv2-S	LVD-142M	self-supervised	142.0	4.9	60.2	39.7	21.6	28.3	31.0
DINOv2-B	LVD-142M	self-supervised	142.0	3.2	41.9	21.9	16.0	19.3	20.5
DINOv2-L	LVD-142M	self-supervised	142.0	2.0	21.2	10.9	10.7	11.4	11.3
DINOv2-G	LVD-142M	self-supervised	142.0	1.9	13.4	8.1	10.7	9.6	8.7
SWIN-L-384	IN1k	supervised	1.2	3.6	18.0	36.0	25.6	17.4	20.1
SWINv2-L-384	IN21k+IN1k	supervised	14.0	3.2	9.5	17.0	24.9	16.4	14.2
ConvNext-L	IN21k+IN1k	supervised	14.0	4.6	31.8	21.2	13.9	19.9	18.3
YOLO11m-cls	IN1k	supervised	1.2	10.0	85.0	78.8	30.2	52.1	51.2
ViT-MAE	IN1k	self-supervised	1.2	21.4	90.4	89.1	60.5	56.9	63.7
DINOv1-ViT-B-16	IN1k	self-supervised	1.2	10.7	71.9	69.2	24.8	35.5	42.4
PaliGemma3b	many	self-supervised	22256.0	7.5	66.7	51.1	19.5	32.2	35.4
BEIT-B-16-224	IN21k+IN1k	self-supervised	14.0	5.0	45.7	44.5	20.7	18.9	26.9
BEIT-L-16-224	IN21k+IN1k	self-supervised	14.0	3.3	35.5	32.9	15.3	12.8	20.0
BEITv2-B-16-224-1K-1K	IN1k+IN1k	self-supervised	1.2	4.1	30.9	34.0	28.7	19.6	23.5
BEITv2-B-16-224-22K-1K	IN1k+(IN21k+IN1k)	self-supervised	14.0	4.0	24.4	29.0	15.5	16.8	17.9
SIGLIP-SO400-14-384	WebLI	contrastive	22000.0	5.6	40.4	23.2	15.0	23.8	21.6
SIGLIP2-SO400-14-384	WebLI	contrastive	22000.0	3.6	35.9	20.5	12.6	16.7	17.9
SIGLIP-B-16-224	WebLI	contrastive	22000.0	10.4	44.3	55.5	27.3	37.5	35.0
SIGLIP2-B-16-224	WebLI	contrastive	22000.0	8.6	49.4	54.8	24.8	32.5	34.0
NaN	NaN	NaN	3652.0	8.0	49.0	45.2	23.0	26.2	30.3

Table 15: Raw attack success rates (%). QG is QuickGELU, Training procedures are supervised (S), self-supervised (SS), and contrastive (C).

Model Name	Training Dataset	Training Procedure	Training Dataset Size (M)	Random				GeometricMasksV1			GeometricMasksV2					COCO Objects			ImageNet-C Distortion Severity				
				Random Hue 0.5	Random Saturation 0.9	Random Contrast 0.9	Random Brightness 0.7	Circle 50	Circle 80	Circle 110	Circle 140	3-4-2 C1 Opacity 64	3-4-2 C1 Opacity 96	3-4-2 C1 Opacity 128	3-4-5 C1 Opacity 128	3-7-2 C1 Opacity 128	6-4-2 C1 Opacity 128	6-7-2 C1 Opacity 128	Black Background	Threshelded Perlin Noise Background	Perlin Noise Background	ImageNet-R	1	2	3	4	5
ResNet50	IN1k	S	1.2	14.6	2.3	2.8	10.0	40.5	83.7	97.7	99.6	33.7	62.1	92.2	87.7	99.1	99.0	99.6	18.3	18.6	22.3	56.5	16.4	26.9	36.9	50.9	65.4
ViTB-16-224	IN21k+IN1k	S	14.0	18.8	4.2	6.6	16.7	15.1	29.4	55.0	83.4	23.8	40.3	58.5	51.5	80.6	90.4	88.1	24.3	25.5	36.0	50.2	7.1	14.4	20.8	33.0	50.1
ViTB-32-384	IN21k+IN1k	S	14.0	16.8	3.7	5.5	15.4	24.1	55.3	85.0	97.7	16.3	33.8	58.6	53.2	94.5	88.1	98.4	21.0	23.8	32.7	52.7	8.7	16.1	22.2	35.3	52.1
ViTL-16-384	IN21k+IN1k	S	14.0	12.8	2.8	4.6	11.8	16.8	39.0	69.0	91.1	14.2	21.9	33.0	31.2	52.8	66.6	89.2	15.0	17.6	29.2	42.6	7.7	13.1	17.7	26.8	41.3
ViTL-32-384	IN21k+IN1k	S	14.0	19.4	4.7	7.4	16.5	23.9	51.8	83.3	97.5	18.5	34.5	57.7	52.1	89.0	85.4	98.5	20.8	24.4	35.7	49.3	7.7	14.3	19.5	30.1	46.1
CLIP-ViTB-16	DFN-2B	C	2000.0	16.0	3.6	4.3	13.8	18.3	39.7	65.5	86.6	18.3	27.8	38.8	40.5	64.8	66.4	78.9	20.5	22.8	27.6	15.3	12.1	22.5	30.8	43.3	57.7
CLIP-ViTB-32-QG	OPENAI-WIT	C	400.0	27.5	7.6	9.4	20.8	36.0	62.1	83.2	95.3	41.7	56.1	68.3	70.5	90.7	89.5	95.5	28.5	37.8	41.2	26.7	12.8	23.1	32.8	47.0	62.4
CLIP-ViTB-32-QG	LAION-400M	C	413.0	25.8	7.1	9.4	21.8	27.3	53.8	78.8	94.1	39.0	58.4	80.4	76.9	93.3	96.2	92.8	30.3	36.7	41.6	20.4	15.5	26.6	35.9	49.7	64.2
CLIP-ViTB-32	LAION-2B	C	2000.0	23.9	6.6	7.7	19.5	27.9	55.2	80.9	95.1	34.2	52.4	69.0	68.4	91.8	89.9	94.8	29.4	33.8	36.8	19.5	15.0	25.8	35.0	48.4	63.1
CLIP-EVA02-B-16	LAION-2B(1.6B)+ COYO-700M(400M)	C	2000.0	16.2	3.6	4.6	12.8	19.8	40.5	65.5	88.4	20.5	29.7	40.0	44.4	69.0	71.0	83.5	18.6	19.9	23.4	17.0	8.2	16.1	23.6	34.7	49.7
CLIP-ViTL-14-QG	MetaClip-400M	C	400.0	16.1	4.1	6.1	15.0	23.2	43.2	63.8	83.0	17.2	22.7	28.8	30.8	43.1	48.8	69.0	20.5	22.0	27.5	9.5	10.4	18.7	25.8	37.9	
CLIP-ViTL-14-QG	OPENAI-WIT	C	400.0	17.0	3.6	5.1	12.6	25.6	43.3	60.5	78.2	18.9	25.5	32.4	36.4	43.7	46.3	68.9	16.5	22.6	28.8	11.0	8.7	15.6	21.9	32.1	45.5
CLIP-ViTL-14	DataComp-1B	C	1400.0	13.4	2.7	3.3	10.5	17.4	35.6	58.0	80.9	15.8	22.4	28.7	29.3	42.3	44.6	67.7	16.0	17.9	23.2	7.8	7.2	13.2	18.8	28.3	40.8
CLIP-ViTL-14	MetaClip-full CC	C	2800.0	14.5	3.5	5.3	13.8	18.8	35.3	55.6	77.3	14.1	19.6	25.8	26.8	37.0	51.3	72.7	19.0	21.0	24.0	8.3	8.5	16.1	22.0	32.4	45.5
CLIP-ViTL-14	DFN-2B	C	2000.0	10.8	2.2	3.1	9.7	15.0	35.5	63.2	87.7	11.2	18.4	27.3	28.4	47.5	53.2	79.0	16.4	17.9	21.4	9.0	6.7	13.5	19.3	28.7	41.6
CLIP-EVA02-L-14	LAION-2B(1.6B)+ COYO-700M(400M)	C	2000.0	11.5	2.3	3.5	8.7	11.6	24.9	44.9	69.8	10.1	15.2	21.8	22.3	34.2	42.4	62.2	13.6	15.8	17.2	6.3	5.4	9.4	13.2	19.4	29.6
CLIP-ViTH-14	DFN-5B	C	5000.0	8.7	1.9	2.7	8.7	11.8	30.9	59.6	86.8	8.9	15.3	24.2	24.1	52.6	64.8	87.4	14.4	16.2	20.9	6.9	6.4	12.2	17.5	26.0	39.3
DINOv2-S	LVD-142M	SS	142.0	7.0	1.9	2.1	8.7	20.2	47.9	77.7	95.0	13.2	17.4	26.3	26.3	50.9	53.5	90.1	17.4	21.3	26.2	40.7	9.2	17.2	24.9	37.0	53.3
DINOv2-B	LVD-142M	SS	142.0	4.3	1.3	1.3	6.1	11.4	26.7	51.7	77.8	7.5	9.3	12.6	12.7	22.9	28.2	60.2	12.9	17.5	17.6	30.0	6.0	11.1	16.2	24.9	38.4
DINOv2-L	LVD-142M	SS	142.0	2.5	0.9	0.8	4.0	5.7	11.6	23.8	43.6	4.4	5.2	6.4	7.0	10.6	11.5	31.1	9.4	12.0	10.7	19.4	3.6	6.7	9.2	14.2	23.4
DINOv2-G	LVD-142M	SS	142.0	2.1	0.8	0.8	3.8	4.7	8.0	14.4	26.6	3.8	4.6	5.8	6.1	8.6	9.8	18.3	8.2	13.2	10.8	17.9	3.3	6.1	7.9	11.7	19.0
SWINv2-L-384	IN1k	S	1.2	7.2	1.2	1.4	4.7	8.2	11.7	19.5	32.5	9.6	12.3	15.8	17.6	67.6	53.6	75.3	8.6	26.8	41.5	31.2	7.6	11.1	15.5	21.3	31.5
SWINv2-L-384	IN21k+IN1k	S	14.0	6.7	0.9	1.1	3.9	6.8	8.8	10.2	12.2	5.8	6.7	7.9	8.2	25.8	17.6	47.2	8.1	30.1	36.4	29.7	7.1	11.0	14.6	19.7	29.4
ConvNext-L	IN21k+IN1k	S	14.0	7.7	2.2	2.4	6.2	13.7	25.9	37.8	49.6	8.2	11.4	15.9	20.6	18.7	30.2	43.2	12.1	12.7	16.9	32.6	8.2	13.4	17.5	24.7	35.5
YOLO1 1m-cls	IN1k	S	1.2	16.0	4.0	4.5	15.5	50.4	90.8	98.9	99.7	31.7	58.8	82.0	91.6	97.7	91.3	98.7	21.7	30.0	38.9	57.4	25.4	39.6	51.7	65.9	77.8
ViTMAE	IN1k	SS	1.2	33.6	8.3	13.7	30.0	68.5	94.4	99.0	99.6	58.8	81.2	92.8	94.9	98.7	98.0	99.2	46.5	54.6	80.6	76.3	30.3	45.5	56.9	69.9	81.7
DINOv1-ViTB-16	IN1k	SS	1.2	13.2	6.7	6.7	16.1	30.1	66.4	92.2	98.9	29.5	46.7	63.0	63.2	90.6	92.4	98.9	19.5	22.8	32.2	61.6	11.7	21.9	32.7	47.4	63.8
PaliGemma3b	many	SS	22256.0	11.5	2.5	3.9	12.2	26.1	59.5	84.7	96.5	17.1	26.5	38.5	46.2	68.3	69.8	91.4	16.2	19.3	23.0	15.1	11.0	20.5	29.6	42.5	57.5
BEIT-B-16-224	IN21k+IN1k	SS	14.0	10.1	1.4	1.8	6.7	12.7	29.9	56.9	83.2	13.2	21.3	31.1	34.5	67.0	71.0	73.2	16.7	17.4	27.8	36.6	6.5	11.3	15.9	23.9	37.0
BEIT-L-16-224	IN21k+IN1k	SS	14.0	6.5	1.0	1.0	4.6	8.9	20.5	41.8	71.0	8.6	12.4	17.2	17.4	42.4	63.1	69.0	11.4	13.2	21.2	26.3	4.6	7.9	10.5	15.6	25.4
BEITv2-B-16-224	IN1k+IN1k	SS	1.2	7.7	1.2	1.5	5.8	11.0	19.7	34.5	58.4	8.8	12.9	17.9	19.6	32.4	77.9	68.7	9.8	15.1	61.1	35.2	7.7	12.1	17.4	24.6	36.2
BEITv2-B-16-224	IN1k+IN21k+IN1k)	SS	14.0	7.9	1.1	1.3	5.5	7.0	11.5	24.5	54.4	5.7	9.4	20.7	18.5	29.8	49.9	69.0	10.8	11.8	23.9	30.8	6.6	11.2	14.5	20.7	31.1
SIGLIP2-SO400-14-384	WebLI	C	2200.0	8.5	1.8	3.3	8.9	13.0	28.1	48.7	71.7	7.9	11.8	16.5	18.9	27.9	28.8	50.4	12.0	14.7	18.2	5.1	7.7	14.4	20.9	31.3	44.7
SIGLIP2-SO400-14-384	WebLI	C	2200.0	6.3	1.4	2.0	4.5	11.8	24.0	42.0	65.9	9.3	12.1	16.0	16.2	24.6	22.0	43.1	9.8	13.4	14.7	4.0	4.3	8.7	13.8	22.3	34.6
SIGLIP-B-16-224	WebLI	C	2200.0	15.3	3.8	6.5	16.1	12.8	28.0	54.7	81.8	22.2	34.1	47.7	48.1	79.1	73.7	83.1	23.9	26.0	32.0	8.0	14.0	25.8	36.0	48.8	63.1
SIGLIP2-B-16-224	WebLI	C	2200.0	14.1	3.4	5.0	11.9	15.8	34.7	61.8	85.4	23.1	35.1	47.7	46.6	76.6	74.5	79.9	21.1	25.1	28.4	8.8	11.0	21.7	30.5	42.7	56.7
Average			3652.0	13.1	3.1	4.2	11.5	19.8	39.1	59.6	77.7	17.9	27.4	38.0	38.6	57.4	61.4	75.5	17.8	22.0	29.1	27.1	9.7	17.1	23.6	33.7	46.8